Electronic state dependence in dissociation of core-excited water

Christian Stråhlman

June 1, 2011

Degree project (Master of Science), 30 hp

Supervisor: Anna Sankari

Division of Synchrotron Radiation Research
Department of Physics

LUND UNIVERSITY
Faculty of Science

Abstract

Water (H_2O) is the most studied molecule in the history of science. Yet many things remain unknown about its nuclear motion and decay. In recent years some studies have been made on the behavior of core-excited water molecules and its subsequent Auger decay and dissociation. Particular attention has been drawn to the ultra-fast dissociation channel $H_2O^* \rightarrow H + O^*H$, which occurs on a femtosecond time-scale in the $H_2O^*(O1s^{-1}4a_1^1)$ core-excited state.

This study concerns the outcome of an electron energy resolved electron–ion coincidence (PEPICO) measurement on core-excited H_2O. The experiments were carried out at the I411 beamline at the MAX II synchrotron in Lund. A setup consisting of a time-of-flight ion spectrometer and an electron energy analyser was used to measure the energy of Auger electrons in coincidence with the resulting ion fragments from the decay. Although this method implies intriguing features, issues concerning false coincidences and detector resolution leave room for improvement. The report discusses possible improvements of the experimental method and data analysis.

We verify that ultra-fast dissociation channels exist, and we are able to directly observe the associated Auger decay $O^*H \rightarrow OH^+ + e^-$ in coincidence with the OH^+ ionic fragments. In the same Auger electron energy region we study the spectator Auger decay to anti-bonding H_2O^+ electronic states. We find a state-specific effect where the intermediate state $H_2O^*(O1s^{-1}2b_2^1)$ has a strong preference for decay to states dissociating to $OH + H^+$, whereas $H_2O^*(O1s^{-1}4a_1^1)$ predominantly dissociates to $OH^+ + H$.

Acknowledgments

To write a master thesis is a process. It starts in a stable ground state where you are confident in your present knowledge and skills; transforms to an intermediate excited state governed by great confusion and chaos; and ends in a final state of even greater knowledge and understanding. I am very grateful to those who have contributed to this project and this report, in all of its states, both practically and spiritually.

First and foremost I wish to sincerely thank my supervisor Anna Sankari. Your interest in my project, your firm and clear guidance and your willingness to discuss both scientific and practical matters regularly has been absolutely essential to the finalization of this report. Especially I thank you for contributing with the computer calculations presented in this report.

I would like to express my gratitude to all the other members of my research group; Stacey Sorensen, Matheiu Gisselbrecht, Joakim Laksman and Erik Månsson, for your support in this project, for a good scientific discussion and for letting me participate in your experiments and in daily work of the group.

I am grateful to Anna Sankari, Joakim Laksman, Stacey Sorensen, Rami Sankari (MAX-lab), Leena Partanen and Antti Kettunen (both from University of Oulu) who performed the experiments presented in this report. A special thanks to Edwin Kukk (Universty of Turku) who introduced me to the experimental setup and provided the data analysis tools needed for PEPICO, and to Rami Sankari who has provided additional information about the spectrometer resolution.

My thanks to the staff and diploma workers at the Division for Synchrotron Radiation Research who have been the best of colleagues and have created a creative atmosphere at the Division.

Finally, thanks to those who gave me a helping hand reading and proof-reading this report, especially Sara Andersson. Also I would like to mention my friends at the Lund Social Sciences Student Union and the Student Union for Humanities and Theology who gave of their time to discuss physics with me. Your contributions to the popular summary were very helpful.

Contents

1 Introduction

Water is perhaps the most studied substance in the history of science. Its importance for life on Earth cannot be over–emphasized. All chemical processes important for life take place in aqueous solution. The importance of water was stressed already by the ancient Greek natural philosophers. Starting with Empedocles (492-432 BC.) water was suggested to be one of the four fundamental elements in nature [1]. The theory of the four elements was the standard dogma for nearly two thousand years. During the 19th century it became evident that water was a substance made up by small molecules consisting of even smaller atoms. The discovery of quantum mechanics in the early 20th century provided a theory which could explain molecular bonding and the interaction between molecules. To this day molecular physicists and physical chemists are exploring what quantum mechanics can tell us about the structure of all matter around us.

The interaction between light and the H_2O molecule is of particular interest. It has been suggested that bio-molecules on Earth might have originated from photo-induced chemical reactions in water solution. Besides these obvious biological implications we know that interactions of light with molecules in the atmosphere has great significance, and gives rise to both the ozone layer and the greenhouse effect. It has been suggested that photo–induced reactions with water might be a future source of hydrogen gas [2]. For these reasons it is of great interest to study the dissociation processes in water.

This report describes and discusses a study on a special case of fragmentation, namely dissociation of the H_2O molecule after irradiation by X-rays with specific energies. This approach allows us to study the behavior of the molecule when it is in certain electronic states. Energetic X-rays induce an energy surplus to the molecule, known as a core–hole state. Methods to evaluate the structure and dynamics of such states have been developed during the last two decades, especially connected to the rapid development of synchrotron radiation instrumentation [3]. Studies of nuclear motion and dissociation patterns in core–excited small molecules have been plentiful. Also studies of gas-phase water (vapour) have been published. Of particular interest has been extremely rapid dissociation channels where fragmentation of the molecule takes place within a few femtoseconds, the same time-scale as molecular vibrations. Also, how vibrational motion in core–excited molecules affects the final states has gained interest [3]. These studies provide us with increasing knowledge of the exotic intermediate core–excited state, and give us growing insight to the very nature of the chemical bonds that keeps our world together.

The purpose of this study is, in particular, to investigate how excitation to different core–excited states affects the outcome of the de-excitation. We wish to clarify the probable and possible decay channels of the water molecule. This will be done by applying an electron–ion coincidence mechanism where we combine a measurement of the energy of emitted electrons, with a count of the resulting ionic fragments. Our hopes are that these methods combined are more powerful than they would be by themselves.

2 Theory

2.1 The molecule

A molecule is held together by molecular bonds which can be described by electronic wave functions. For a stable molecular bond it is necessary that it is energetically favorable for two atoms to be close to each other. To understand why molecules break their bonds and dissociate one must explore the nature of these bonds and why they are formed.

2.1.1 The quantum description of molecules

If one wishes to gain a complete understanding of a molecule, one would have to solve the time-independent electronic Schrödinger equation,

$$\mathscr{H}_e \Phi(\mathbf{r}) = E\Phi(\mathbf{r}), \tag{1}$$

with the electronic Hamiltonian $\mathscr{H}_e$ taking into account the movement of n electrons in the electric field created by N nuclei and the interaction of all the electrons and nuclei with each other. Such a Hamiltonian has the form (in atomic units[1])

$$\mathscr{H}_e = \sum_{i=1}^{n} \frac{-\nabla_i^2}{2} + \sum_{i}^{n}\sum_{A}^{N} \frac{-Z_A}{r_{iA}} + \sum_{i}^{n}\sum_{j>i}^{n} \frac{1}{r_{ij}} + \sum_{a}^{N}\sum_{B>A}^{N} \frac{Z_A Z_B}{R_{AB}}. \tag{2}$$

Solving the time-independent Schrödinger equation analytically is impossible for each molecule with more than three constituent particles[2]. A molecule has both a complicated electric field created by the nuclei, and many intrinsic degrees of freedom since the nuclei can move in respect to each other. From a mechanical perspective the fundamental addition of complexity arises from the possibility for the molecule to change its intrinsic framework due to nuclear motion. In a stable molecule this can be treated as two types of periodic motion: Rotation — where the whole nuclear framework is rotating — and vibration — where the nuclear framework is changing shape. Rotation and vibration, in addition to electronic transitions, makes the molecular quantum mechanical system far more complex than the atomic case [4, p. 383f].

A great simplification to the understanding of molecular structure is the *Born–Oppenheimer approximation*. It relies on the fact that nuclei are heavier than electrons by at least a factor of thousand, and the electric forces governing their motion are the same order [4, p. 383]. Nuclei are thus much slower than electrons. As a consequence, it is reasonable to consider nuclei to be fixed during electronic transitions. Also, we can rely on the electrons to adapt to a change in the nuclear framework almost instantaneously [5, p. 258]. During a vibrating motion of the nuclei, where the internuclear distance may change, the electronic wave functions will adapt instantaneously.

Rotational, vibrational and electronic transitions are not independent. However, when considering the associated energy, rotational transitions often require the least energy. Vibrational transitions require more energy than rotational transitions. Electronic transitions require more energy than vibrational transitions [5, p. 338]. The

[1] Atomic units is a system of units suitable for atomic calculations. It arises when four fundamental constants of nature is defined to unity. These constants are the electron mass, the elementary charge, the reduced Planck's constant and Coulomb's constant.

[2] The only molecule with three constituent particles is the hydrogen molecular ion H_2^+

pure rotational spectrum of the water molecule is observed in far infra-red [6][7]. The fundamental vibrational frequencies are observed in near infra-red and extend up into the visible spectrum [8]. The electronic transitions considered in this report range from a few electron volts (visible spectrum) to hundreds of electron volts. The rotational motion leads to a second-order splitting in a molecular spectrum, whereas the vibrational motion itself leads to a first order splitting [4, p. 385f]. The rotational levels are energetically too close to each other to have any measurable effect on the result of the dissociation process, thus they will not be further discussed. Vibrational splitting is however visible in some electron spectra found in this report.

The Born–Oppenheimer approximation implies that for a given arrangement of atomic nuclei, the solutions of the Schrödinger equation will be a set of wave functions

$$\Phi_1(\mathbf{r}), \Phi_2(\mathbf{r}), \Phi_3(\mathbf{r}), \ldots$$

associated with a set of discrete energies

$$E_1, E_2, E_3, \ldots$$

Movement of a nucleus will result in an immediate change of these functions. Thus, if one has two nuclei in free space constituting a diatomic molecule, one can plot the energy eigenvalues as a function of the internuclear distance R, thus one will have the functions $E_1(R), E_2(R), \ldots$. The Born–Oppenheimer approximation allows us to present the results as a function of nuclear distance. These functions are called *potential curves*. Potential curves are illustrated in *figure 1*. All potential curves have the common characteristic that $E_n(R) \to \infty$ when $r \to 0$, because the nuclei will repel each other if they get closer. Also, $E_n(R) \to E_\infty$ when $r \to \infty$, which is the energy of the two separated atoms [5, p. 260]. The potential curves of molecules will be of much importance when determining the possible electronic transitions in molecules.

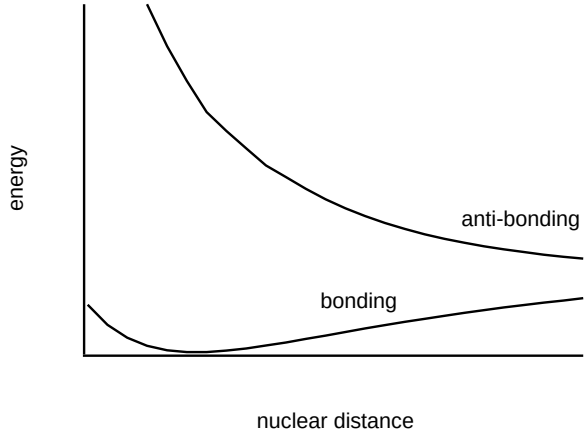

FIGURE 1 – *Potential curves corresponding to bonding and anti-bonding states.*

The minimum of the lower potential curve in *figure 1* explains the existence of molecular bonds. Undisturbed nuclei will arrange themselves in a state with minimum energy. If the potential curve has a minimum there exists an equilibrium

distance where the molecular system has the lowest possible energy. Such a state is known as *bonding*. States without minima can be either *anti–bonding* or *non–bonding*. For evaluation of dissociation these states are important to distinguish, since molecules put in anti–bonding or non-bonding states will dissociate.

2.1.2 Symmetry

Of fundamental importance for the molecular orbital theory are the concepts in the mathematical framework of *group theory*. In particular, group theory well explains the mathematics behind symmetric properties of objects. Symmetry is very important in everyday life. Even if one may not notice, very many man-made objects carry at least one symmetric property. An object is said to hold a symmetry when we can define a transformation of the object which, when executed, leaves the object seemingly unchanged [9, p. 2]. These properties can also be applied to molecules like H_2O.

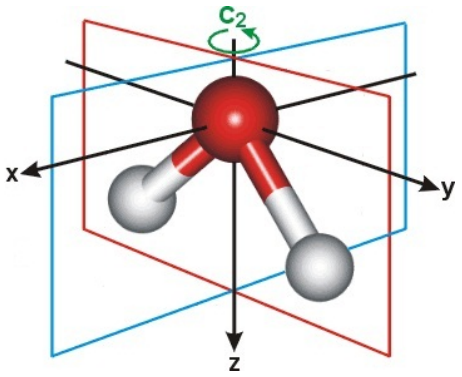

FIGURE 2 – *The symmetric species of the* H_2O *molecule, including one* C_2 *rotational axis and two mirror planes. (Picture: Martin Chaplin)*

A molecule is a quantum mechanical system described by wave functions in space and time. These wave functions must be expressed within a defined coordinate system. If the molecule carries a symmetry property it is useful to define the origin at a point coinciding with an inversion point, a rotational axis or a mirror plane. The center of mass is always a suitable choice. In H_2O one can place it almost in the center of the oxygen atom, due to the large difference in mass of oxygen and hydrogen. As illustrated in *figure 2* the water molecule has a rotational axis (label: z-axis) with 2-fold rotational symmetry, which means that one can rotate it 180° around the axis an abritrary number of times and still leave it unchanged. It has also two mirror planes - the xz-plane and the yz-plane. A water molecule can thus be defined as a *point group* with well defined symmetric properties. The H_2O molecule belongs to a point group called C_{2v}. Here C_2 denotes rotational symmetry without inversion symmetry. v should be interpreted as symmetry through mirror planes *vertical* to the xy-plane. It should be noted that the bent "Mickey Mouse"-shape of H_2O makes it different from linear tri-atomic molecules, e.g. CO_2 , with D_∞ symmetry. If H_2O had been linear it would have completely different properties due to symmetry effects, including non-polarity and different vibrational modes.

Symmetry considerations must be undertaken when constructing molecular or-

bitals. The symmetry properties of a point group are contained in the *irreducible representations* in a character table. The character table for the C_{2v} is presented in *table 1*. Each irreducible representation corresponds to a *symmetry species*. For C_{2v} there exist four symmetry species — A_1, A_2, B_1, B_2. The character table for C_{2v} can be used to find the symmetric properties of H_2O.

C_{2v}	E	C_2	$\sigma_v(xz)$	$\sigma_v'(yz)$	
A_1	1	1	1	1	z, z^2, x^2, y^2
A_2	1	1	-1	-1	xy
B_1	1	-1	1	-1	x, xz
B_2	1	-1	-1	1	y, yz

TABLE 1 – *The character table for the C_{2v} point group. Each row corresponds to a symmetry species arising from a irreducible representation. The charachters decribe the behavour of a symmetry species under a symmetry operation. E.g. one can see that the identity symmetry operation E (the act of doing nothing) has the result 1 for each symmetry species. The object remains unchanged. However for the rotation symmetry operation C_2 only the A symmetry species remain intact while B symmetry species are inverted. The $\sigma_v(xz)$ and $\sigma_v'(yz)$ are reflections in the respective planes. The functions to the right describe which functions that are associated to the irreducible representation. If e.g. an object transforms like xz it can be represented by* B_1.

A note should be made on the labelling system. The labels, called Mulliken symbols [10], describe the behavior of the symmetry species under symmetry operations. Some wave functions in symmetric molecules will stay intact under symmetry operations (symmetric) while others change sign (anti-symmetric). These are labeled as follows:

A_1 is symmetric with respect to rotation around the principal rotational axis and symmetric with respect to a vertical mirror plane perpendicular to the principal axis.

A_2 is symmetric with respect to rotation around the principal rotational axis and anti-symmetric with respect to a vertical mirror plane perpendicular to the principal axis.

B_1 is anti-symmetric with respect to rotation around the principal rotational axis and symmetric with respect to a vertical mirror plane perpendicular to the principal axis.

B_2 is anti-symmetric with respect to rotation around the principal rotational axis and anti-symmetric with respect to a vertical mirror plane perpendicular to the principal axis.

This notation will be used for the H_2O molecule. For OH in point group $C_{\infty v}$ the story is a bit different. Because of its infinite number of possible rotations around the principal axis (which is directed along the molecular bond) it makes no sense to talk about an anti-symmetric rotation. Instead one must define an infinite set of degenerate B-states and denote them E_n where $n \in \mathbb{N}$. Because the $C_{\infty v}$ point group has a strong connection to the full rotation group R_3 of free atoms, there is

also a strong connection to LS-notation. In analogy a $\Lambda\Sigma$-notation has been adopted for linear molecules. here $A_1 = \Sigma^+$, $A_2 = \Sigma^-$. Non-rotationally-symmetric states (degenerate E-states) are labeled $\Pi, \Delta, \Phi, \ldots$ in analogy with $P, D, F, \ldots$ in atoms.

2.1.3 Construction of molecular orbitals

Just as electronic wave functions in atoms form atomic orbitals, electronic wave functions in molecules form molecular orbitals. To evaluate these from the molecular electronic Hamiltonian in *eqn. 2* is a tedious task which cannot be carried out the same way as it can for atoms. Within the Born–Oppenheimer approximation this will be mathematically complex even for small molecules. One can, however, simulate molecular orbitals as a linear combinations of constituent atomic orbitals. This technique is known as *molecular orbitals as linear combinations of atomic orbitals (LCAO)* [4, p. 400]. The molecular orbitals ϕ are written as

$$\phi = \sum_r c_r \chi_r$$

where χ_r are atomic orbitals and c_r are numerical factors. The atomic orbitals used constitute a basis set for the calculation [5, p.262]. In principle one can find the solutions by applying *variational theory*. Essentially one will find molecular orbitals by applying some constraints arising from energy and symmetry considerations. First, the binding energies of the atomic orbitals must be similar to contribute to molecular orbitals [5, p. 269]. Hence, for the bonds between O and H atoms one will only find molecular orbitals combing H1s with O2s, $O2p_{x,y,z}$. Secondly, the orbitals must have a constructive overlap[3].

The O1s orbital is too compact and located too close to the nucleus to overlap. An overlap can only be constructive if the orbitals have the same symmetry [14, p. 5]. With these considerations one can construct molecular orbitals for H_2O and OH.

The hydroxide molecule OH belongs to the $C_{\infty v}$ symmetry. The basis set is the O and H atomic orbitals.

$$\phi = c_1\chi(\mathrm{H1s}) + c_2\chi(\mathrm{O1s}) + c_3\chi(\mathrm{O2s}) + c_4\chi(\mathrm{O2p_x}) + c_5\chi(\mathrm{O2p_y}) + c_6\chi(\mathrm{O2p_z}) \quad (3)$$

The principal nuclear axis, by convention, is z. Hence H1s, O1s, O2s and $O2p_z$ belong to the Σ symmetry species. The O1s is left undisturbed. The remaining orbitals combine to three σ–orbitals. $O2p_x$ and $O2p_y$ belong to Π symmetry species and cannot overlap with H1s. Thus they form undisturbed π–orbitals. The orbital occupation of OH in its ground state is

$$1\sigma^2 2\sigma^2 3\sigma^2 1\pi^3.$$

This suggests that the molecular orbitals will be constructed as follows:

$$\begin{aligned}
\phi(1\sigma) &= \chi(\mathrm{O1s}) \\
\phi(n\sigma) &= c_1\chi(\mathrm{H1s}) + c_3\chi(\mathrm{O2s}) + c_6\chi(\mathrm{O2p_z}) \\
\phi(1\pi) &= c_4\chi(\mathrm{O2p_x}) + c_5\chi(\mathrm{O2p_y})
\end{aligned}$$

Since all electrons except one are paired in doubly occupied orbitals the unpaired electron makes an overall $^2\Pi$ state.

[3] An overlap is where two wave functions partly occupy the same region in space. When they do, they both contribute to the overlap integral. If the overlap integral is positive, the overlap is constructive.

The water molecule is trickier due to its bent shape. It belongs to the C_{2v} symmetry. The basis set is the same as for OH with the addition of one more H1s.

$$\begin{aligned}\phi =& c_1\chi(\mathrm{H1s_A}) + c_2\chi(\mathrm{H1s_B}) + c_3\chi(\mathrm{O1s}) + \cdots \\ &\cdots + c_4\chi(\mathrm{O2s}) + c_5\chi(\mathrm{Op_x}) + c_6\chi(\mathrm{Op_y}) + c_7\chi(\mathrm{Op_z}).\end{aligned} \tag{4}$$

Now the z–axis is directed along the C_2 rotational axis as in *figure 2*. One can assign the O orbitals to the four symmetry species of the group $(\mathrm{a_1}, \mathrm{a_2}, \mathrm{b_1}, \mathrm{b_2})$, but the H1s orbitals ($\mathrm{H1s}_A$ and $\mathrm{H1s}_B$) do not by themselves belong to a symmetry species (they are not symmetrical with regard to the rotational axis). It is therefore necessary to form *symmetry–adapted linear combinations* to get at suitable basis set. Since the H1s orbitals are equvivalent, one can construct two virtual orbitals as linear combinations of the H1s orbitals.

$$\begin{aligned} c_A\chi(\mathrm{A_1}) &= c_1\chi(\mathrm{H1s_A}) + c_2\chi(\mathrm{H1s_B}) \\ c_B\chi(\mathrm{B_2}) &= c_1\chi(\mathrm{H1s_A}) - c_2\chi(\mathrm{H1s_B}) \end{aligned}$$

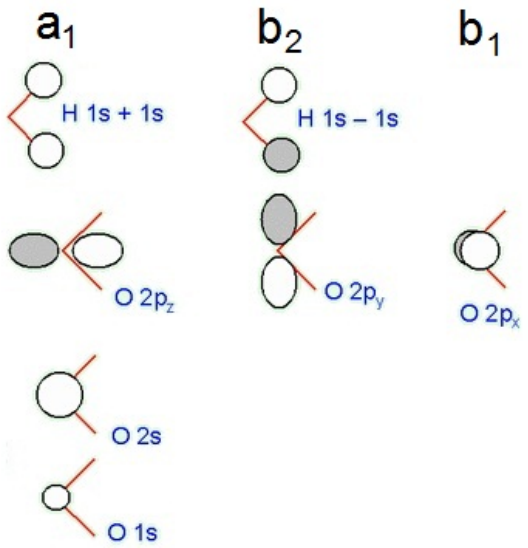

FIGURE 3 – *SALC-orbitals for* $\mathrm{H_2O}$. *Assigments has been made to the symmetry species. (Picture: Jeremy Harvey)*

It is obvious from the graphical representation in *figure 3* that $\chi(\mathrm{A_1})$ and $\chi(\mathrm{B_2})$ belong to the $\mathrm{A_1}$ and $\mathrm{B_2}$ symmetry species. As before the O1s is left undisturbed. The remaining orbitals are characterized according to their symmetry species, which suggests that the molecular orbitals will be constructed as follows [5, p. 274]:

$$\begin{aligned} \phi(1\mathrm{a_1}) &= \chi(\mathrm{O1s}) \\ \phi(n\mathrm{a_1}) &= c_A\chi(\mathrm{A_1}) + c_4\chi(\mathrm{O2s}) + c_7\chi(\mathrm{O2p_z}) \\ \phi(1\mathrm{b_1}) &= \chi(\mathrm{O2p_x}) \\ \phi(n\mathrm{b_2}) &= c_B\chi(\mathrm{B_2}) + c_6\chi(\mathrm{O2p_y}) \end{aligned}$$

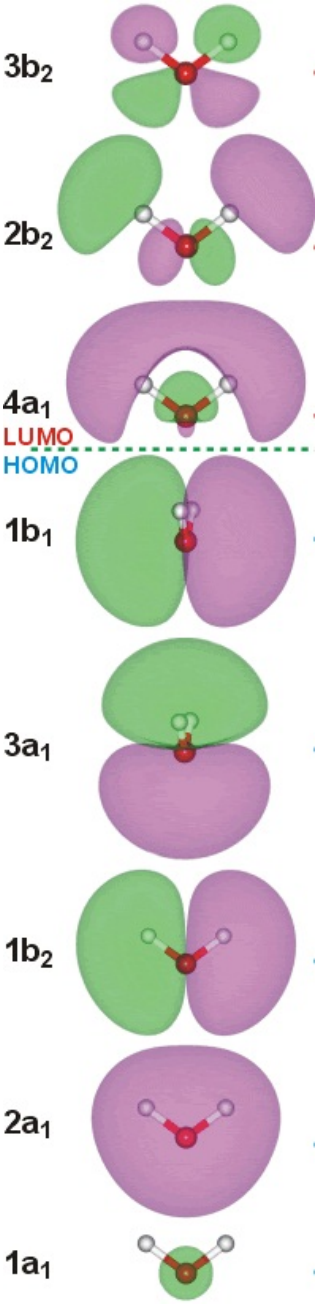

FIGURE 4 – *The resulting molecular orbitals from a LCAO calculation on* H_2O. *HOMO denotes the highest occupied molecular orbital* $1b_1$ *and LUMO the lowest unoccupied molecular orbital* $4a_1$. *Note that the graphical representation of* $3a_1$ *and* $1b_1$ *is rotated 90°. (Picture: Martin Chaplin)*

To find the order of the orbitals one has to solve a secular equation for each of the symmetry species [5, p. 275]. The result is seen in *figure 4*. The 10 electrons of H_2O in its ground state occupy orbitals

$$1a_1^2 2a_1^2 1b_2^2 3a_1^2 1b_1^2.$$

Since all electrons are paired in doubly occupied orbitals the state is $^1A_1$. Above the occupied orbitals one finds the un-occupied orbitals $4a_1$ and $2b_2$.

2.2 Decay and dissociation

The aim of this report is to study the dissociation processes of core-excited H_2O. This requires an understanding of how a core-excitation can be induced, how the molecule may decay from its excited state, and under what conditions molecular bonds may break.

2.2.1 Interaction of light with the molecule

Our knowledge of how light induces excitations in molecules arises from their absorption spectra. An absorption spectrum of H_2O acquired by Hjelte et al [2] is shown in *figure 5*.

When a molecule is irradiated with light it may absorb a photon and its energy. The energy of the molecule is then increased from the initial state energy E_i to the final state energy E_f. If no ionization is induced, as will happen when the photon energy is higher than the ionization energy, the energies must fulfill the energy conservation relation

$$h\nu = E_f - E_i \tag{5}$$

where $h\nu$ is the photon energy. In practice this means that a photon can only be absorbed if there exists a final state with a suitable energy. The absorption peaks thus indicate photon energies which are probable to induce excitations.

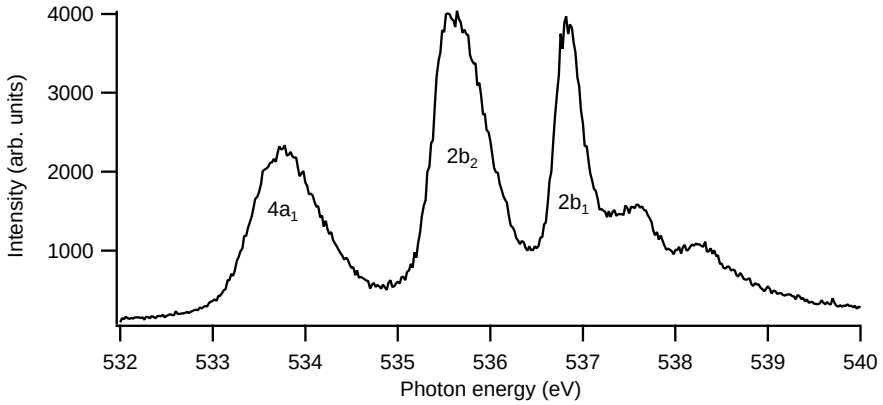

FIGURE 5 – *Absorption spectrum of* H_2O *indicating the transitions. E.g.* $4a_1$ *here indicates the transition* $O1s \rightarrow 4a_1$ *explained in the text. The classification of the three most prominent peaks is well known [2][12][13]. (Data obtained by the Hjelte et al [2] during the experiment described in the publication.)*

On absorption of a photon an electron is promoted from a filled molecular orbital to an unoccupied orbital. Such a state is often unstable and short-lived. The molecule is in an excited state, denoted by a star e.g. H_2O^*. A special case is when an electron in a deep orbital is promoted to an unoccupied orbital. Such a state is called *core-excited*. The H_2O molecule has only one core-orbital, namely O1s. The photon energy region shown is well known to include the photon energies which induce transitions from O1s to unoccupied molecular orbitals [2][12][13]. To decide on the classification of states one must apply calculations of the molecular orbital structure and use symmetry arguments.

Apart from atomic-like core orbitals, the orbitals in molecules are of two types, valence and Rydberg. In the valence case the promoted electron is described to occupy one molecular orbital where there is a strong correlation between the ionic core and the electron. In the Rydberg type of states the electron is treated as it sees the nucleus and all other electrons as one single charged particle [14, p. 8]. This means that they are atomic-like in their structure.

For the experiment this implies that we can choose to excite the molecule to a specific final state if we have a light source with well defined monochromatic light. Such light can be obtained at synchrotron light sources. The required light is in the X-ray regime.

The mathematical treatment of photo-induced transitions is further elaborated in appendix A. It can be shown that the symmetry species of the final orbitals restricts which orbitals can be populated by core-excitation of O1s electrons. *Figure 5* show that transitions to the three first unoccupied orbitals are possible.

2.2.2 The Franck–Condon principle

The implementation of the Born–Oppenheimer approximation also has an effect on the theory of transitions. The Franck–Condon principle states that "because nuclear masses are so much larger than the mass of an electron, an electronic transition occurs within a stationary nuclear framework" [5, p. 388]. Its implication is that each electronic transition will correspond to a vertical movement between two potential curves, as depicted in *figure 6*. The range of nuclear coordinates where a transition can happen is called a Franck–Condon region. Its width is determined mainly by the depth of the potential well of the initial electronic state. A deep well corresponds to a narrow Franck–Condon region

The Franck–Condon principle couples the electronic and vibrational states, since a transition between electronic states determines also which vibrational states are possible to occupy. Vibrational states are only an issue when the excited state is bonding. Excitation to other states leads to dissociation.

2.2.3 Auger decay

An excited state must eventually decay. In light core-excited atoms and molecules the dominant de-excitation channel is *Auger decay* [11, p. 6], the radiationless analog to X-ray emission. A vacancy in the core orbital is filled by a electron in a higher orbital. The released energy is transferred to another electron in a higher orbital which is ejected from the molecule. The molecule thus becomes ionized, so called *autoionization*. The kinetic energy of the ejected electron equals the energy difference of the excited state and the relaxed state. The energy of the ejected electron, called an *Auger electron*, is thus a signature of the energy of the relaxed state in the ionized

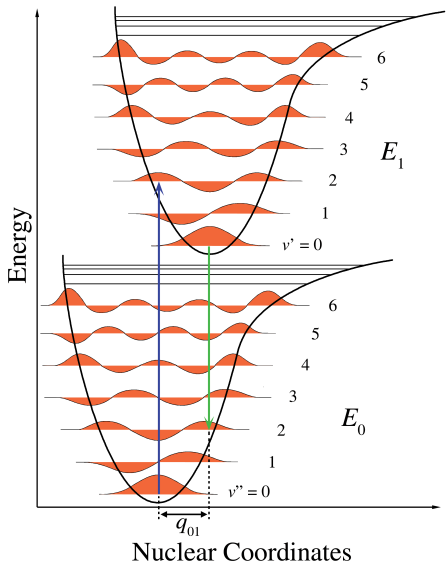

FIGURE 6 – *A transition between an initial state with energy E_0 to a final state E_1 corresponds to a vertical movement between potential curves according to the Franck–Condon principle. A molecule in a certain electronic and vibrational state can thus only be excited within the Franck–Condon region. (Picture: Mark M. Somoza)*

molecule. The energy of the Auger electron is thus not directly dependent on the initial photon energy $h\nu$. If the energy of the excited state is known and the kinetic energy of the ejected electron is measured, the energy of the relaxed state can be calculated. The spectrum of Auger electrons is a measure of the possible electronic states in the ionic molecule.

Figure 7 shows a normal Auger spectrum of H_2O published by Siegbahn et al [15]. Their sample was irradiated by Mg K_α rays ($h\nu$ =1253 eV). The characteristic of a *normal* Auger electron spectrum is that the process is induced by an inner-shell photoionization of the molecule. This is different from *resonant* Auger electron spectrum where the initial excitation is to a specific intermediate state. The spectrum should illustrate the multitude of possible Auger electron energies that originate from a core-excited molecule.

One can make a distinction between two types of resonant Auger decay — participator decay and spectator decay — differing in the orbitals involved in the process.

Consider the excitation of one O1s electron to the $4a_1$ orbital.

$$h\nu + H_2O \rightarrow H_2O^*(O1s^{-1}4a_1^1)$$

One electron fills the vacancy. This could e.g. be one $1b_2$–electron. The energy is transferred to the $4a_1$–electron which is ejected.

$$H_2O^*(O1s^{-1}4a_1^1) \rightarrow H_2O^{+*}(1b_2^{-1}) + e^-$$

This is the participator decay, since the originally promoted electron participates in the Auger decay. The result is an ion with a valence vacancy. (Note that the ion still

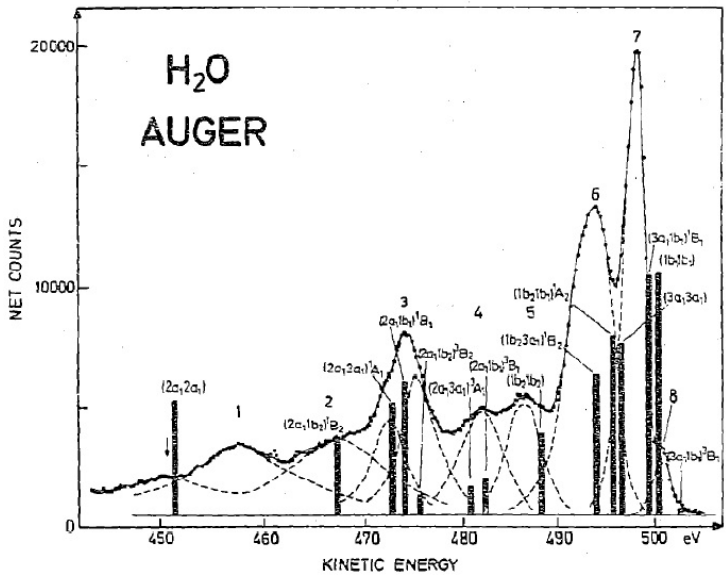

FIGURE 7 – *Normal Auger spectrum following excitation by Mg K_α X-rays. The full line indicate the measured spectrum. The dotted lines and bars indicate an attempt to classify the Auger transitions. The spectrum shows that there is a multitude of Auger processes following excitation by X-rays, most of them with Auger electron energies far lower than 500 eV. (Spectrum from Siegbahn et al [15])*

is excited and can decay further.) The other case would be if the excess energy instead is transferred to another electron e.g. the $1b_1$–electron.

$$H_2O^*(O1s^{-1}4a_1^1) \rightarrow H_2O^{+*}(1b_2^{-1}1b_1^{-1}4a_1^1) + e^-$$

This is the spectator decay, since the originally excited electron does not participate in the Auger decay. The result is an ion with one promoted electron and two valence vacancies.

Each of these H_2O^+ states is associated to a potential curve. The energy of the Auger electron will correspond to the vertical distance between the excited and relaxed state. For that reason a combination of Auger spectra and potential curves allow for a classification of Auger decay channels. This report will further explore these possibilities for H_2O.

2.2.4 Fragmentation patterns for the core-excited water molecule

In the most straightforward case the core-excited H_2O molecule decays to a stable H_2O^+ fragment without more effort than the ejection of an Auger electron. However, the decay pattern shows much greater complexity than that, as can be seen in *figure 8*.

The core-excited H_2O molecule will eventually undergo Auger decay. In the 1990s there was an ongoing discussion about the possible occurance of ultrafast dissociation of the core-excited water molecule [3]. Auger decay of core-excited H_2O takes place on the femtosecond timescale. The ultrafast dissociation is characterized

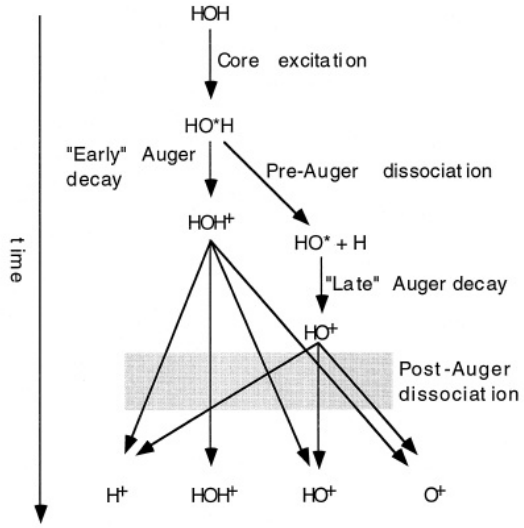

FIGURE 8 – *Fragmentation patterns for core-excited* H_2O. *The complexity arises from a combination of Auger decay and dissociation. Here only singly charged fragments are presented, but neutral and doubly charged species may also occur. (Picture from [12])*

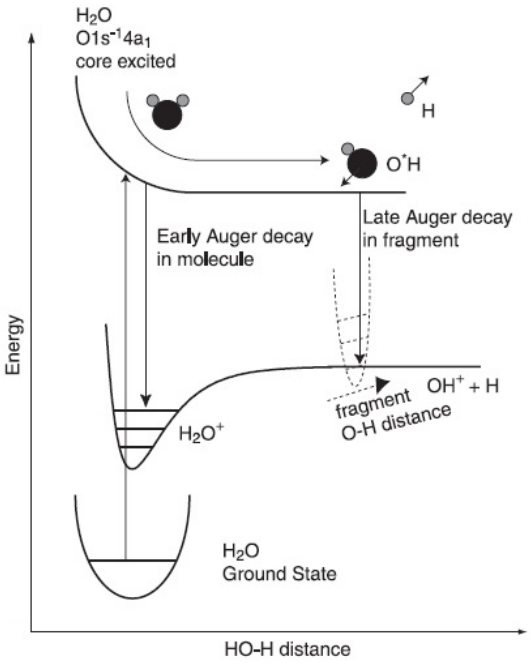

FIGURE 9 – *Schematic and simplified illustration of the early and late dissociation process. The x-axis shows the distance along one* O–H *distance, whereas the other is kept fixed. (Picture taken from [3].)*

by a dissociation on the same time-scale as Auger decay. We call this "late" Auger decay. The process is illustrated in *figure 9*. It had been shown for other molecules that this type of dissociation could occur in strongly dissociative core-excited states. Hjelte et al [2] showed in 2001 that such ultrafast dissociation existed in water.

In early Auger decay the core-excitation is immediately followed by Auger decay.

$$h\nu + H_2O \rightarrow H_2O^* \rightarrow H_2O^{+(*)} + e^-$$

The H_2O^{+*} state can decay by further Auger decay (further ionization) or fragmentation into charged and neutral fragments. In late Auger decay the core-excitation is immediately followed by a pre-Auger fragmentation. The Auger decay takes place within the fragment.

$$h\nu + H_2O \rightarrow H_2O^* \rightarrow OH^* + H \rightarrow OH^{+(*)} + H + e^-$$

Hjelte et al [2] used a very elegant method to find the ultrafast dissociation from high resolution Auger spectra. By a slight detuning of the incident photon beam they could observe an equal detuning in the Auger spectra. This detuning is observed for all early Auger decays where the potential curves in the Franck–Condon region are not parallel (see *figure 9*). A slightly lower photon energy will excite the molecule at a slightly longer O–H distance, and thus the Auger decay will have slightly lower energy. Late Auger decay will occur in a Franck–Condon region where the curves are parallel and thus no detuning will be observed. This method, with pure Auger spectrum analysis, is powerful by its own means. But it has only limited possibilities to give a qualitative and quantitative analysis of the final states reached after decay.

Following the logic of *figure 8*, one can argue that quantitative and qualitative analysis of the decay products can be done by ion detection. An extensive study of this kind has been done by Piancastelli et al [16]. They used a synchrotron light source to scan a sample of water vapour in the same energy region as the absorption spectrum in *figure 5*. They detected the ion yield for each possible outcome ion. Such an experiment can identify the outcome fragments of a core-excitation process. However, it cannot say anything about the actual final states of the fragments and how the electronic configurations play a role in the process.

In a study analogous to their measurements on water, Hjelte et al showed the existence of ultra-fast dissociation in ammonia (NH_3) [17]. In addition to the analysis of Auger spectra they also compared their findings with electron energy resolved electron-ion coincidence measurements. They could show that the $N1s \rightarrow 4a_1$ resonance in NH_3 mainly gave rise to NH_2^+-ions arriving in coincidence with electrons of the kinetic energy of the late Auger process. This was a strong argument since it implied the proposed decay pattern.

$$h\nu + NH_3 \rightarrow NH_3^* \rightarrow NH_2^* + H \rightarrow NH_2^{+(*)} + H + e^-$$

Coincidence measurements can thus prove to be a useful tool to connect the powers of both normal/resonant Auger electron spectroscopy and ion yield measurements. It gives a stronger possibility for identification of individual states. Since in coincidence measurements one can assign fragmentation to certain Auger electron energies, one can thus hopefully determine the fragmentation patterns giving them assignments to final states.

3 Methods

This section describes in brief the method we have used to acquire our data and to analyse it. A more extensive description of the synchrotron radiation and beamline I411 can be found in appendix B. A more detailed description of the PEPICO spectrometer can be found in appendix C.

The strength of electron energy resolved *photoelectron photoion coincidence spectroscopy (PEPICO)* is the ability to simultaneously measure the electron energy of photoelectrons (or other energetic electrons such as Auger electrons) and ions produced by ionization or dissociation. An experimental setup for PEPICO must thus consist of two interconnected parts, one electron spectrometer and one ion detector. There must also be an electronic steering system making sure that the two measurements are connected and stored together.

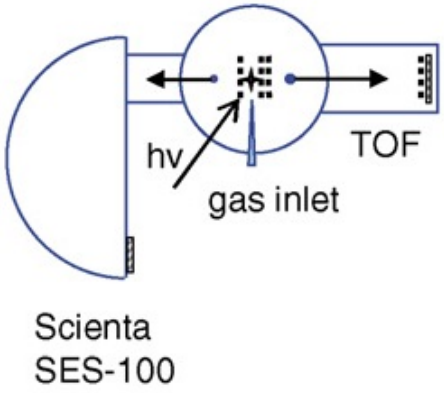

FIGURE 10 – *General composition of the setup viewed along the photon beam. The electron analyser is to the left and the TOF spectrometer to the right. The gas is injected in the chamber through a needle. (Picture from [18])*

The data presented in this report were measured at beamline I411 at MAX-lab (see appendix B) in June 2010 by a joint group from University of Oulu and Lund University[4]. They were acquired using a PEPICO setup designed and described by Kukk et al [18]. It consists of a Scienta SES-100 hemispherical electron analyser and a ion time-of-flight (TOF) spectrometer. Its general features are shown in *figure 10*. A detailed description is given in appendix C. The electron analyser gives, after calibration, the energy of the electron. The ion TOF spectrometer gives the mass-to-charge ratio of the ion. These two parameters are stored together. A measurement is called an *event*. An event where one or more ions are detected with an electron is named a *coincidence*.

The components are mounted perpendicular to the propagation direction of the synchrotron light, as illustrated in *figure 10*. After ionization of a molecule, the emitted electron might be detected in the electron analyser. The electron detection will trigger a pulse leading to the creation of an electric field extracting all cation[5] species

[4]The author did not participate in these measurements. See Acknowledgments for the full list of participants.

[5]A cation is an ion with a positive net charge, i.e. less electrons than protons in the nucleus. A photoelectron or Auger ionization i a free neutral molecule will always produce cations.

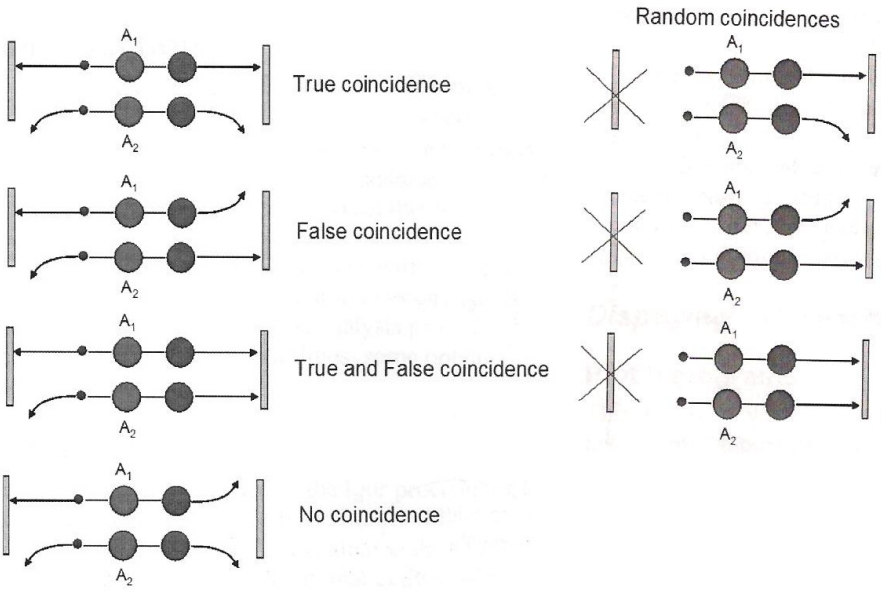

FIGURE 11 – *The left panel shows the possible outcomes of an event in pulsed extraction field mode. We detect the electron coming from ionization A_1. At the same time there is a ionization A_2 which is not detected. We have a true coincidence if the resulting fragment(s) from A_1 are detected and not resulting fragment(s) from A_2. In many events we will however detect false coincidences or no coincidences, either because we do not succeed to extract the right ions, or we do not succeed to extract any ions at all. The right panel shows the possible outcomes of a random coincidence. These are not triggered by an electron detection, and thus necessarily false. (Picture: Edwin Kukk)*

from the extraction region to the TOF-spectrometer. The cations are accelerated by an electric field in the direction of the TOF spectrometer axis. Heavy fragments will arrive at the detector later than light fragments, thus allowing for a separation of different ion species.

If the detected photoelectron and the detected photo-ion were created in the same ionization process it is a true coincidence; otherwise it is a false coincidence. It should be well noted that only a fraction of the coincidences will actually be true. *Figure 11* shows the possible true and false coincidences. To get the best possible data we must deal with the false coincidences that will inevitably occur. In the pulsed extraction field mode we cannot directly separate true and false coincidences. It is simply not possible to deduce if one electron and one ion originate from the same process. Therefore we have to rely on an indirect measure of *random coincidences*. The random coincidences, shown in *figure 11* are artificially generated events where no electron is triggering the detection. The random triggers are governed by a time pulse. All events measured after a random trigger event are necessarily false coincidences. The events after an electron trigger are a mix of true and false coincidences. However, on average, the electron triggered events contain the same ions as the necessarily false, random triggered coincidences plus the true coincidences. Therefore, if we consider the average number of ions $\bar{N}_{co}$ in electron triggered events, and the average number of ions $\bar{N}_{rnd}$ in random events. Then the number of true events will be

$$\bar{N}_{true} = \bar{N}_{co} - \bar{N}_{rnd}. \tag{6}$$

This average random subtraction method can be applied to each bin of TOF events. It can never deduce if a single event is true or false.

The data analysis has been done with a custom made macro in Igor Pro, developed by Edwin Kukk[6]. The datasets used here include some hundred thousand events per resonance. To give a view of the relative sizes of $\bar{N}_{co}$ and $\bar{N}_{rnd}$ the graph in *figure 12* shows the coincident and random TOF spectrum for the fragmentation process following core excitation to the $H_2O^*(O1s^{-1}4a_1^1)$ (hereafter denoted $4a_1$, the label of the intermediate state). It should be noted that a *large majority* of the coincidences recorded are false, in the sense that a large fraction of the events, statistically, do not originate from one single ionization process. The measure of the quality of data is known as *purity* and is defined as

$$100 \cdot \frac{\bar{N}_{co} - \bar{N}_{rnd}}{\bar{N}_{co}} \tag{7}$$

The data presented here has a purity between 10 and 15. This implies that 85-90 percent of all measured coincidence events are false.

Kukk et al [18] have performed tests on the validity of the statistical method with valence electron ion coincidence of rare gases. They note that the method was proven to work effectively at detection rates up to 500 Hz [18]. In the following we have thus stayed below this regime.

The high rate of false coincidences is however a drawback. Significant improvements to the quality of the data are required. The false coincidences appear because we cannot make sure that only one ionization event takes place during one extraction. With reference to *figure 11* this means that all coincidences would be true if

[6]University of Turku, Finland

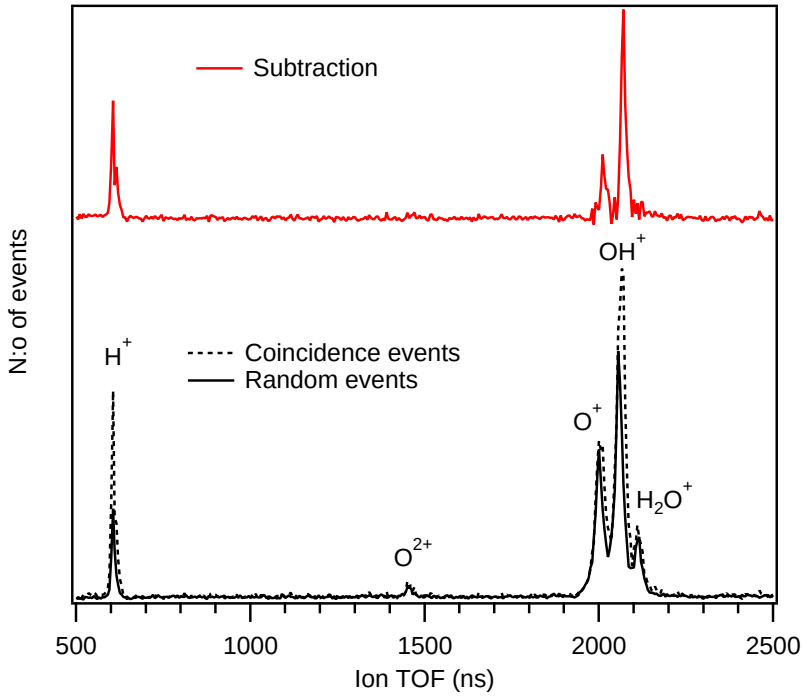

FIGURE 12 – *Sample time-of-flight spectrum for the resonance* $4a_1$. *Here coincidence events* $\bar{N}_{co}$ *and random events* $\bar{N}_{rnd}$ *are shown in an overlay. The resulting TOF* $\bar{N}_{true}$ *from* eqn. 7 *is shown above. Note that two ions,* H_2O^+ *and* O^{2+}, *are visible in the coincidence spectrum but disappears in the subtracted spectrum.*

A_2 would be eliminated. As we have seen in *figure 7* there is a large amount of auto-ionization processes in H_2O where the Auger electron is emitted with an energy lower than our detectable energy region. All auto-ionization involving Auger electrons with low energies will contribute to the false coincidences since unrelated ions will be present in the extraction region. One way around this problem is to lower the rate of events, by decreasing the light intensity or by reducing the number of molecules in the extraction region (lowering the gas-pressure). Of course this increases the time needed for the experiment. To do the opposite, increase the gas-pressure, would probably increase the number of false coincidences, but also increase the number of coincidences overall. This could itself increase the statistical significance of the subtraction.

An issue connected to the resolution of the experiment is the acceptance of the electron analyser. The present setup requires that the electron itself hits the detector. Therefore the acceptance angle should be large to maximize the number of electron triggered events recorded. The drawback here is that the energy resolution of the detector decreases with a high acceptance angle. The data presented here were acquired with a high acceptance. The resolution of the electron analyser under full illumination is 1.6 eV. In practice we cannot get a full illumination, and thus the resolution is estimated to 1.2-1.3 eV. The photon energy resolution of the beamline is 1.1 eV [19]. This could be compared to the resolution of the Auger spectrum of Hjelte et al, which was obtained with 90 meV photon energy resolution and 140 meV electron analyser resolution [2].

Both TOF and electron energy must be calibrated. When it comes to TOF one shall convert TOF into mass-to-charge ratio. One must make use of the relation

$$t = t_0 + C\sqrt{\frac{m}{q}} \tag{8}$$

where t_0 and C are constants to be determined. It takes only two known points to do this, and thus we have chosen to normalize to H^+ and H_2O^+. Identification of each peak is listed in *table 2*.

Fragment	TOF interval
H^+	580 – 640 ns
O^{2+}	1430 – 1490 ns
O^+	1970 – 2030 ns
OH^+	2030 – 2090 ns
H_2O^+	2090 – 2150 ns

TABLE 2 – *Time-of-flight intervals found for each fragments.*

The energy calibration of the electron detector results in a condition that converts distance on the detector plate to energy. We have used two well known photoelectron peaks in Xe 4d spectrum to calibrate [20]. This allows us to calibrate the detector for the energy region 502-512 eV. All data were acquired in this energy region.

4 Results and Analysis

4.1 Evaluation of PEPICO maps

To evaluate the coincidence events one makes use of PEPICO maps. These are two-dimensional graphs with electron energy along one axis and TOF along the other. The map itself is a two-dimensional false-colour histogram. *Figure 13* shows the PEPICO map of the fragmentation process following core excitation to $4a_1$. The map shows the coincidence events marked in a two-dimensional array with Auger electron kinetic energy on the x-axis and ion TOF on the y-axis. Random subtraction has been made, both in the TOF and the false-color map. The map is square-root-scaled to allow for the display of weaker processes.

Three strong horizontal fragment lines are visible. With reference to *table 2* they are assigned to H^+ (bottom), O^+ (middle) and OH^+ (top). Only a weak stroke of H_2O^+ can be observed at 509 eV Auger electron energy. The OH^+ signal dominates the map and shows two peaks at 505 eV and 508 eV. In the former case it is accompanied by a maximum in the O^+ abundance. H^+ fragments are only observed in the lower energy end, with a peak value at 506 eV.

To compensate for the low electron energy resolution we make a comparison to the high resolution Auger spectrum for this and the adjactent energy region. This spectrum is displayed in *figure 14*. The Auger spectrum for $4a_1$ were evaluated by Hjelte et al [2]. They found, as noted above, evidence for early and late Auger decay in the lower energy region. Especially, they observed vibrationally resolved structures at 508 eV and 511 eV which they concluded could only originate from an Auger decay of the core-excited OH fragment, an evidence for late Auger decay. These structures can be observed in *figure 14*. This observation allowed Hjelte et al to conclude that there would exist ultra-fast dissociation of the $4a_1$ state.

Our measurements show a large abundance of OH^+ at 508 eV and above with only small abundances of other fragments, suggesting that the dominating process releases OH^+ and H fragments. This is an observation in support of ultrafast dissociation connected to Auger energies in this region. No large abundances of other charged fragments are observed in this region, suggesting that OH^+ does not dissociate further.

The Auger energies associated to ultrafast dissociation has been assigned by Hjelte et al [2] to $^1\Sigma^+$ and $^1\Delta$ final states in OH^+. They also made a calculation of the transition rates[7] to these states and noted that they would expect a larger rate for $^1\Delta$ than for $^1\Sigma^+$. They also predicted a transition to a $^1\Pi$ state in OH^+ with 508 eV Auger energy, but did not observe it.

In our experiment the largest OH^+ peak is observed at 508 eV. This would instead suggest a higher transition rate for the $^1\Sigma^+$ or $^1\Pi$ final state, which cannot be resolved.

The H^+ peak is largely unaccompanied at 506 eV, but both OH^+ and O^+ are seen in larger abundances at slightly lower energies. We cannot from the PEPICO map deduce if these charged fragments are observed in coincidence with each other. It would require a photoion photoion coincidence analysis (PIPICO) with the coincidence of two fragments. Unfortunately there is not enough data in this measurement to draw any conclusions on this.

It can be seen from *figure 14* that participator Auger decay from $4a_1$ to the three principal bonding states in H_2O^+ cannot account for the Auger electrons observed

[7] The transition rate is a measure of the probability for a certain transition.

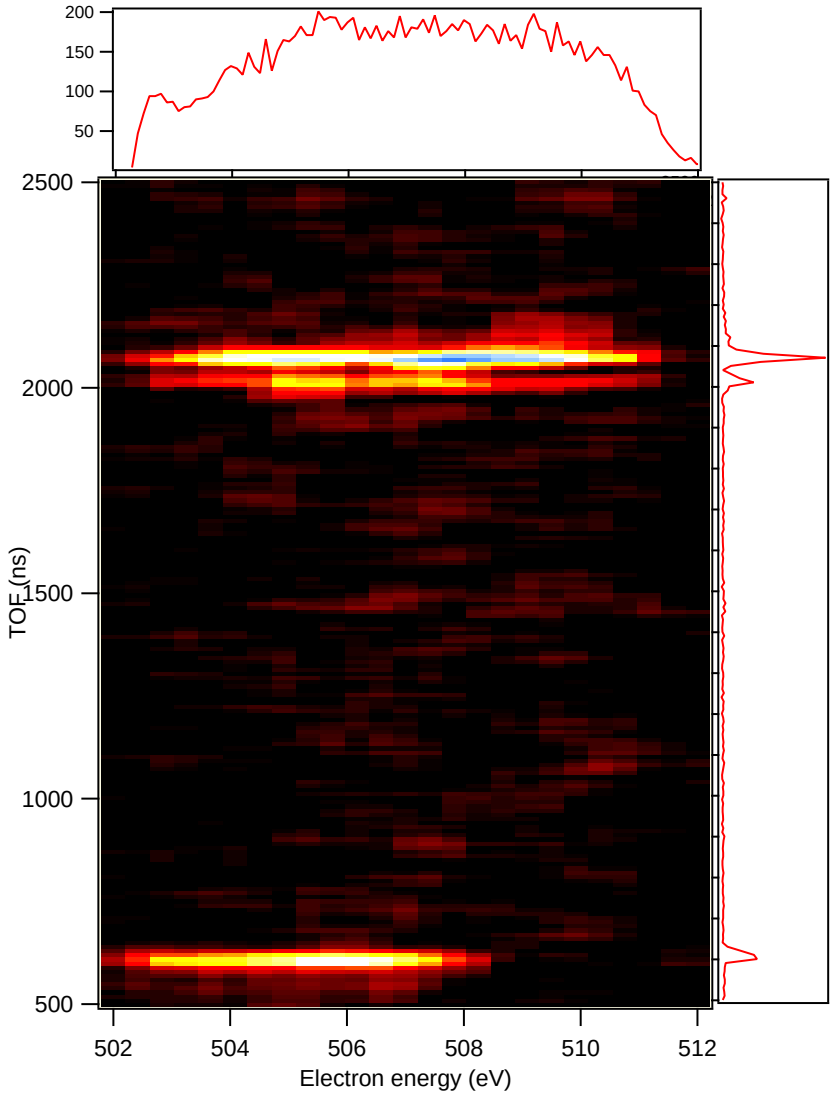

FIGURE 13 – *PEPICO map for the Auger decay from* $4a_1$ *resonance.*

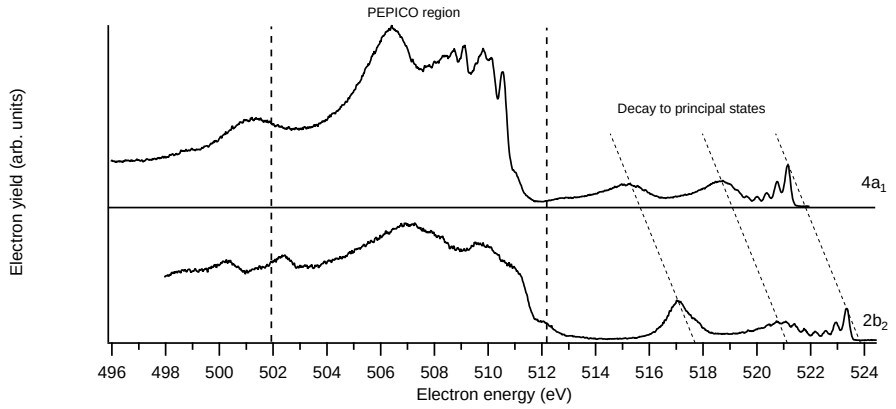

FIGURE 14 – *Auger spectrum with higher resolution measured by the authors of* [2]. $4a_1$ *is shown on top and* $2b_2$ *in bottom. There is no relation of their relative intensity. The region where our PEPICO measurements have been performed is marked. The participator Auger decay to the three principal states* $H_2O^+(1b_2^{-1})$, $H_2O^+(3a_1^{-1})$ *and* $H_2O^+(1b_1^{-1})$ *are highlighted above the PEPICO region. The general increase in electron energy for* $2b_2$ *corresponds to the increase in energy of the excited state.*

in our energy region. The large number of "false" H_2O^+ ions in the TOF spectrum are most likely associated to Auger electrons in the higher energy range. As a consequence all H_2O^+ ions dissappear from the subtracted spectrum.

As noted before, an extensive study of the photo-fragmentation of core-excited H_2O has been published by Piancastelli et al [16]. They measured the partial non-coincident ion yield following core-excitation from photon irradiation in the 531-541 eV region. At $4a_1$ they observed also other fragments, in small abundances. Our experimental conditions have not allowed us to record these ions. One should note that our experiment does not show evidence for O^{2+} in this energy region. The dissociation patterns involving O^{2+} may therefore have other associated Auger electron energies.

Figure 15 shows the PEPICO map of the fragmentation process following core excitation to $2b_2$. Because of the bonding character of $2b_2$, we are not expecting fast dissociation and no late Auger decay. The probable decay pattern is

$$H_2O^* \rightarrow H_2O^{+(*)} + e^-$$

with later dissociation to smaller fragments. *Figure 15* shows a strong H^+ peak at 508 eV. Weaker abundances of O^+ and OH^+ are observed over the whole energy region.

It should be noted that we do not observe any evidence for H_2^+ fragments in the TOF spectrum. Piancastelli et al observed that H_2^+ is weakly produced in $2b_2$ and not in $4a_1$. This feature is often explained by the geometry of the core-excited states, where the $2b_2$ state has a high probability to have bending vibration, where the H atoms may come close to each other [13].

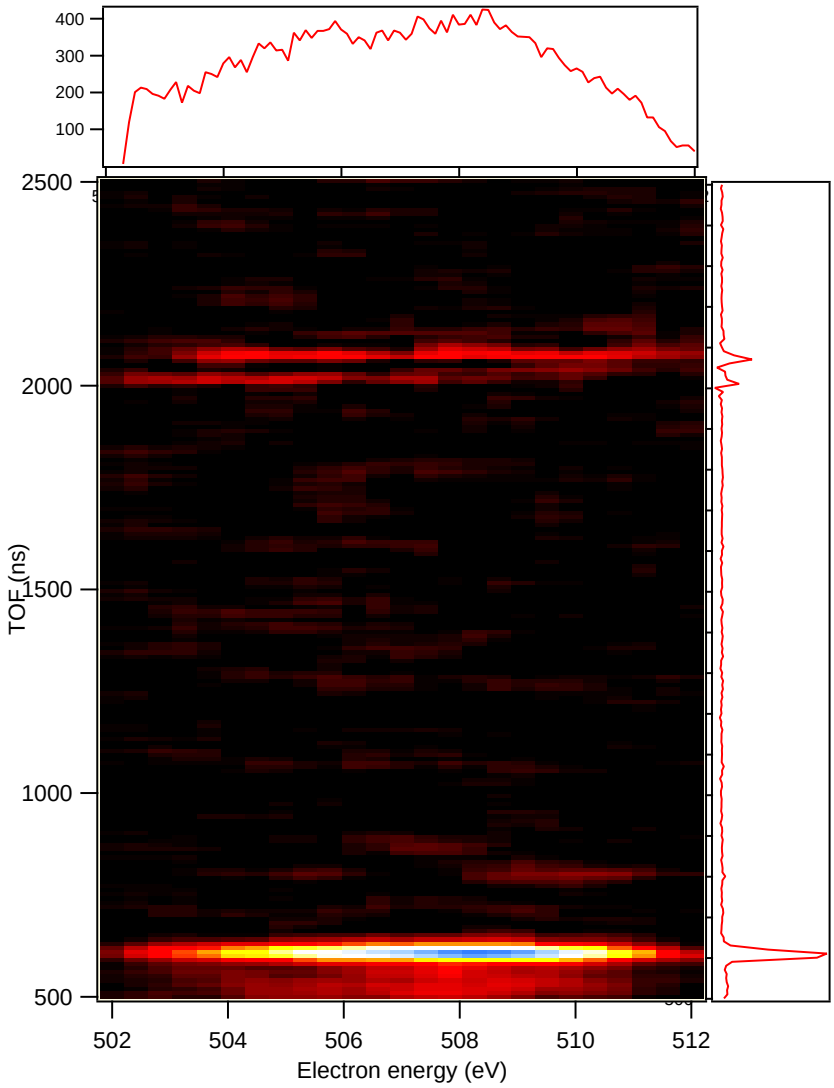

FIGURE 15 – *PEPICO map for the Auger decay from* $2b_2$ *resonance.*

4.2 Calculation of potential curves

To be able to identify the Auger electron energies of the possible transitions we have made calculations of the initial, intermediate and final states[8]. These calculations have included H_2O, H_2O^+ and $(H + OH)^+$ [9]. In *figure 16* all calculated potential curves are presented. The H_2O ground state is presented for reference and for the possibility to identify the Franck–Condon region of the initial core-excitation. It is well established [4] that the equilibrium O–H distance in the H_2O molecule is 0.95 Å. The core-excited H_2O^* states are $4a_1$ and $2b_2$. Note that they in *figure 16* have an 500 eV offset to allow for good comparison with other curves. Curves for the cationic states H_2O^+ and $(H + OH)^+$ are shown in red.

The calculation is based upon a few constraints. The overall nuclear framework depends on the two O–H distances and the H–O–H angle. The one-dimensional potential surface shows the changing of one O–H distance. The other two parameters are kept to their H_2O ground state equilibrium positions 0.95 Å and 105°.

A calculation of the potential curves of OH^+ has also been performed. In practice the calculation has been made on the $(H + OH)^+$ complex where one H is placed at a distance where it is considered to be dissociated (2.5 Å). The other distance is then varied as above. In *figure 16* the $(H + OH)^+$ fragment curves are plotted to the right.

One can view excitation followed by Auger decay relaxation as a set of movements in the potential curves, as we saw in *figure 9*. According to the Franck–Condon principle all electronic transitions are vertical. Following the absorption of a photon, we have a movement vertically in the graph from the H_2O ground state to the core–excited state. The Franck-Condon region is considered to be 0.9-1.0 Å. *Figure 16* suggests that the $4a_1$ state is anti–bonding while $2b_2$ is bonding, which is in accordance with previous studies. The Auger decay will be a vertical transition from a neutral state (black line) to a cationic state (red line). The expected Auger electron energy can be calculated from the difference of energy between an intermediate and a final state.

The three lowest states of the H_2O^+ ion are the principal bonding states, while the three upper calculated states are anti-bonding. A classification has been made on the symmetry species of the states [13]. The distorted H_2O^+ ion is within the C_s point group.

In *table 3* some transition energies have been extracted from *figure 16*. To account for the dissociative character of $4a_1$ we can expect a transition at any separation. 0.9 Å and 1.0 Å mark the borders of the Franck–Condon region. The fragments can be viewed as totally separated at 2.5 Å, whereas any decay at higher separation must be considered to be a transition in a separated OH fragment. Energies for 1.5 Å are given to indicate a possible semi-late decay, i.e. decay during the dissociation.

A closer inspection of the energies associated to the Franck–Condon region shows the different characters of the principal bonding states $1A''$, $1A'$ and $2A'$; compared to the anti-bonding states $3A'$, $2A''$ and $3A''$. The former have a well defined transition energy in the Franck–Condon region, while the latter have their transition energy smeared out over a wider energy range. The bonding curves are thus almost parallel to the $4a_1$ curve in the Franck–Condon region. In comparison with the Auger

[8] The computer calculations of the potential curves presented here have been provided by Anna Sankari. The graphical representations and identification of states have been performed by the author

[9] This notation indicates that we have H and OH separated, but its positive charge is not localized or with unknown location.

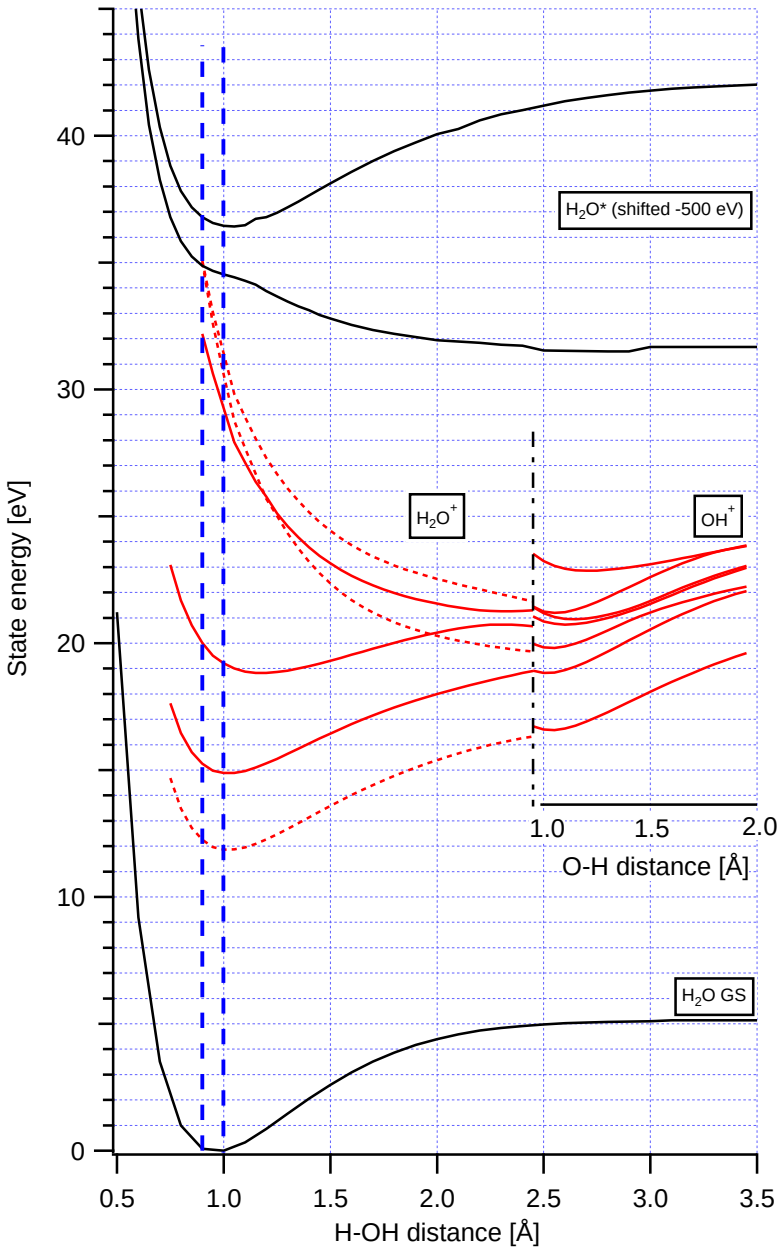

FIGURE 16 – *Calculated potential curves for* H_2O. *The bottom line (black) marks the* H_2O *ground state and the two upper lines (black) mark* $H_2O(O1s^{-1}4a_1^1)$ *and* $H_2O(O1s^{-1}2b_2^1)$. *To allow for a better comparison the core-excited curves have been shifted downwards 500 eV. The six lowest* H_2O^+ *states are shown in red. Here full lines denote A' symmetry and dotted lines A" symmerty within the* C_s *point group (classification from [13]). The box shows the ten lowest calculated states for the* $(H + OH)^+$ *combination with a free* H. O-H *distance in the* OH *fragment is shown along the added x-axis.*

$R_{\mathrm{H-OH}} =$	0.9 Å	1.0 Å	1.5 Å	2.5 Å
$4a_1 \rightarrow 1A''$	522,6 eV	522,7 eV	519,2 eV	515,1 eV
$4a_1 \rightarrow 1A'$	519,6 eV	519,7 eV	516,4 eV	512,6 eV
$4a_1 \rightarrow 2A'$	514,9 eV	515,3 eV	513,5 eV	510,9 eV
$4a_1 \rightarrow 3A'$	502,7 eV	505,3 eV	509,7 eV	510,2 eV
$4a_1 \rightarrow 2A''$	499,9 eV	504,0 eV	510,4 eV	511,9 eV
$4a_1 \rightarrow 3A''$	499,8 eV	503,1 eV	508,4 eV	510,0 eV

TABLE 3 – *Expected Auger electron energies from the decay from* $4a_1$ *to the calculated* H_2O^+ *states shown in* figure 16. *The energies are given for four possible separations of one* O–H *distance. The first two columns are within the Franck–Condon region of the* H_2O *ground state.*

spectrum (*figure 14*) this would imply that the principal peaks are narrower than the associated peaks in the lower energy range. The calculations implies an overlap of Franck–Condon transitions in the energy region 500–505 eV, while semi-late Auger decay will be associated to Auger electron energies in a slightly higher energy range. It should therefore not be possible to distinguish the outcomes of these anti-bonding orbitals. In the Auger spectrum and PEPICO maps we should observe a broad structure.

The anti-bonding $3A'$, $2A''$ and $3A''$ final states of H_2O^+ dissociate along the potential curve to $(H + OH)^+$, with the charge located on one fragment. It is of interest whether they will dissociate into $OH + H^+$ or $OH^+ + H$. To evaluate this additional calculations of the charge distribution in different states of the $(OH + H)^+$ complex[10] have been performed in MOLCAS [22]. We have found that $2A''$ has possibilities to decay into $OH + H^+$ as well as $OH^+ + H$. $3A'$ and $3A''$ shows a preference for dissociation to $OH^+ + H$. Since *figure 13* shows a large peak for H^+ at 506 eV the question is whether $2A''$ can account for this. Its transitions shown in *table 3* suggests that this is possible and that $2A''$ could account for Auger electrons observed in this energy region.

$R_{\mathrm{H-OH}} =$	0.9 Å	1.0 Å	1.1 Å
$2b_2 \rightarrow 1A''$	524,5 eV	524,6 eV	524,5 eV
$2b_2 \rightarrow 1A'$	521,6 eV	521,6 eV	521,5 eV
$2b_2 \rightarrow 2A'$	516,8 eV	517,3 eV	517,5 eV
$2b_2 \rightarrow 3A'$	504,6 eV	507,2 eV	509,4 eV
$2b_2 \rightarrow 2A''$	501,8 eV	505,9 eV	508,8 eV
$2b_2 \rightarrow 3A''$	501,7 eV	505,0 eV	507.6 eV

TABLE 4 – *Expected Auger electron energies from the decay from* $2b_2$ *to the calculated* H_2O^+ *states shown in* figure 16. *Three separations of one* O–H *distance are given. The Franck–Condon region of the* H_2O *ground state is 0.9-1.0 Å and for the intermediate* $2b_2$ *state it is 1.0-1.1 Å.*

In *table 4* some expected Auger energies for $2b_2$ have been drawn from *figure 16*.

[10]The calculation is based on a nuclear framework with one O-H distance at equilibrium 0.95 Å and one H separated from O with 2.5 Å distance.

We are not expecting ultrafast dissociation due to the bonding properties of $2b_2$. *Table 4* thus only give values within the Franck–Condon region. It should be noted however that the $2b_2$ intermediate state has a higher equilibrium separation[13], which can be clearly seen in *figure 16*. Therefore, we consider the Franck–Condon region to be approximately 1.0-1.1 Å.

We also know from earlier experimental and theoretical work [13] that the equilibrium bond angle for $2b_2$ is smaller than for $4a_1$. This implies nuclear movement without dissociation before Auger decay, both in terms of increasing separation and reducing bond angle.

Just as for $4a_1$ the principal bonding states are well defined, while the anti-bonding states show broad energy ranges within the Franck–Condon region. Our calculations show that there is one H_2O^+ anti-bonding state, namely $2A''$, which has a possibility to decay with a release of H^+. *Table 4* indicate Auger decay with energies 505,9 eV to 508,8 eV in the H_2O^+ Franck–Condon region. This is in good agreement with the experimental H^+ peak at 508 eV. It is very plausible that the abundance of H^+ originates from this decay. The smaller abundances of OH^+ can be accounted for with reference to $3A'$ and A'', though no clear peaks can be observed.

One can note that all OH^+ fragment curves in *figure 16* are bonding. It is thus not expected that these states will dissociate further. Instead one would expect a multitude of vibronic states covering Auger energies energies from 515 eV and down. It should be noted that the calculations suggest that OH^+ has a larger equilibrium nuclear separation than H_2O in its ground state. Our calculations show a possibility for the OH^* fragment to decay to OH^+ and release Auger electrons with energies close to 508,5 eV and 510,5 eV.

5 Discussion

5.1 Observations

Studies of molecules with electron energy resolved photoelectron photoion coincidence spectroscopy can give much knowledge of fragmentation processes. In this report the fragmentation patterns of core-excited H_2O molecules have been studied. With a combination of experimental data and theoretical calculations of potential curves we have been able to identify specific fragmentation processes associated with Auger electrons in the energy span 502-512 eV. Energy resolved PEPICO is a powerful tool to combine the powers of pure Auger electron spectroscopy and ion detection. Though powerful, it is also a method inclined to many difficulties, and there is significant capacity for improvement in the methodology.

The Auger electron energy region has been shown to be associated with two classes of dissociation processes. First, we have seen that Auger decay in the Franck–Condon region of the core–excited molecule leads to dissociating H_2O^+states. Second, we have verified that there exists an ultra-fast dissociation channel in the $4a_1$ state, with $H + OH^+$ as its final state signature.

Ultra-fast dissociation of water has been known for some time. Its existence has been proved through high resolution Auger electron spectroscopy. In our study, we have been able to directly observe the ultra-fast dissociation process of $4a_1$ core-excited H_2O by its signature final state dissociation pattern $H + OH^+$. Together with the Auger spectrometric measurements done by Hjelte et al [2], we are thereby able to confirm that Auger electrons in the vicinity of 510 eV are associated to ultra-

fast dissociation. We can however not rule out that fragmentation processes other than ultra-fast dissociation also may be present.

The electron energy resolution in our measurement is low. We have seen from calculations that early and late Auger decay are qualitatively different. Decay from OH^* to bonding states in OH^+ will show up as narrow peaks with vibrational structure. Transitions H_2O^* to anti-bonding H_2O^+ are broader since the potential curves are less parallel. With higher electron energy resolution there would be a possibility to note quantitative differences in the processes. In the present situation, we cannot rule out that there are overlapping dissociation channels which cannot be resolved. Because of this deficiency, we have not been able to assign the Auger energies to specific final states. There are indications that the relaxed OH^+ fragments populate the $^1\Delta$, $^1\Sigma^+$ and $^1\Pi$ states proposed by Hjelte et al [2], but the observed structure is too broad to make a clear designation.

There are large differences when it comes to the decay products of $4a_1$ and $2b_2$. The proposed geometries of the intermediate core-excited states are different, where the bond angle of $2b_2$ is narrower. From $2b_2$ we have observed a strong preference for H^+ fragments over other cations. Since we are expecting almost all $2b_2$ core-excited states to decay via H_2O^+, we thus expect these states to have a preference for dissociation into $OH + H^+$. The calculations we have performed have verified that there is a possible fragmentation channel.

Other studies have reported traces in ion yield measurements of other fragments than those we have observed. We note especially that weak channels such as H_2^+ and O^{2+} in coincidence are not observed. TOF spectra of random triggered events suggests that O^{2+} fragments are produced in some decay channel(s) following core-excitation, but we cannot associate this to any Auger electron energy in the region of interest.

Measurements, particularly in $4a_1$, have shown a multitude of dissociation fragments at certain Auger energies. Regrettably, the data acquired has not been sufficient to make an ion–ion coincidence analysis. Such analysis could give further clues on fragmentation patterns with more than one charged fragment, if such channels exist.

5.2 Enhancement of experiment and analysis

As noted earlier this analysis is based on datasets with quite low purity, which must lead to a discussion on the possible improvements of the experiment and data analysis. The present statistical errors are hard to disregard.

The electron detection resolution in the PEPICO setup is too low to allow us to make clear designations of states in the present study. The low detection resolution is a consequence of the high acceptance we have used in the analyser. A high acceptance has been a necessity to get an acceptable detection rate. To increase the resolution it could be necessary to lower the detection rate and the number of events. The electron detector is run in a specific energy interval, and a narrower interval increases the resolution. However, this might cause a considerably lower amount of detected electrons and thus no real improvement of the detection resolution.

PEPICO studies combined with high resolution Auger electron spectroscopy have been fruitful for this project. Although this is not a measure which will give the full power of PEPICO, it gives important clues on possible decay channels.

One uncertainty connected to the dataset is that only the limited range 502-512 eV has been evaluated. It would be expected that many false coincident ions originate from processes connected to Auger electrons with higher and lower energies.

Transitions from core-excited states to bonding states in H_2O^+ are expected to give H_2O^+ fragments. No H_2O^+ fragments have been observed in the 502-512 eV region, although random triggered events gave rise to these. A measurement in the 512-530 eV region could verify this assumption and give further statistical certainty to the measurements in the lower region.

The hope for improvement might lie in a more evolved statistical analysis including also other datasets than electron triggered coincidences in one energy region. The false coincidences in *figure 11* are of many kinds. Our drawback is that we have no data on the relative weight of the different false channels. We also lack knowledge of the relative weight of the channels which we are not detecting, i.e. where we can not observe the electron. We can suspect that some events are not recorded since the Auger electrons are in the wrong energy region. Some electrons in the right energy region are not recorded either. The statistical analysis could probably be improved if such relative weights could be quantified.

One could, for reference, obtain a total electron yield spectrum in coincidence with ions. This would give a general picture of which other real fragmentation processes occur after core-excitation. With a carefully constructed statistical method this could improve the analysis. The outcome of such manipulations will however be much dependent on the character of the false coincidences, and their relative weight. To further improve the statistics, analysis of the false coincidence channels must be performed.

A Appendix: Symmetry effects in photon induced core-excitations

It is well known that there is a selectivity in the core excitation process. Linearly polarized light will be preferably absorbed by those molecules having the excited orbital aligned to the polarization axis. Thus, a core excitation tends to give an excited molecule with a definite symmetry and orientation [21].

In the mathematical framework a transition occurs when the molecule system undergoes a change from an initial state $|i\rangle$ to a final state $|f\rangle$. The transition is described by an interaction Hamiltonian $\mathscr{H}_I$. The probability for a transition is expressed by a matrix element

$$P_{if} \propto |\langle f|\mathscr{H}_I|i\rangle|^2 \tag{9}$$

The matrix element is primarily a measure of the size of the overlap of the initial and final wavefunction. For photon-absorption the transition probability can be expressed within the dipole approximation as

$$P_{if} \propto |\mathbf{e}\cdot\langle f|\mathbf{r}|i\rangle|^2 \tag{10}$$

where $\mathbf{r}$ is the electron position vector and $\mathbf{e}$ is the vector for the direction of the light polarization. One can immediately deduce that the transition probability will be strongly dependent on the direction of the photon polarization when the light is linearly polarized.

For a transition to be "dipole allowed", the matrix element in *eqn. 10* must necessarily be non-zero. To explore the matrix element one can use symmetry considerations. The matrix element is an integral of the form

$$\langle f|\mathbf{r}|i\rangle = \int \phi_f^* \mathbf{r}\phi_i \,\mathrm{d}\tau. \tag{11}$$

It can be shown mathematically [5, p. 156f] that if the integrand is not a basis for the totally symmetric irreducible representation of the group, then the integral is necessarily zero. For H_2O in the C_{2v} group this means that the integrand $\phi_f^*\mathbf{r}\phi_i$ must span A_1.

Since this report only concerns core-excited states the initial state is always the ground state $|A_1\rangle$. The removed electron is a localized O1s electron in a a_1 orbital. A core hole does thus not affect the overall symmetry of the excited state. The position vector $\mathbf{r}$ can be decomposed to its three components (x, y, z). Each component has a symmetry species according to the character table in *table 1*.

$$x \rightarrow B_1 \qquad y \rightarrow B_2 \qquad z \rightarrow A_1 \tag{12}$$

It remains to determine the symmetry of the integrand of the final states $|A_1\rangle$, $|A_2\rangle$,

$|B_1\rangle$ and $|B_2\rangle$; for each direction in space. In total twelve matrix elements:

$$\begin{aligned}
\langle A_1|x|A_1\rangle &\rightarrow A_1 \times B_1 \times A_1 = B_1 \\
\langle A_1|y|A_1\rangle &\rightarrow A_1 \times B_2 \times A_1 = B_2 \\
\langle A_1|z|A_1\rangle &\rightarrow A_1 \times A_1 \times A_1 = A_1 \\
\langle A_2|x|A_1\rangle &\rightarrow A_2 \times B_1 \times A_1 = B_2 \\
\langle A_2|y|A_1\rangle &\rightarrow A_2 \times B_2 \times A_1 = B_1 \\
\langle A_2|z|A_1\rangle &\rightarrow A_2 \times A_1 \times A_1 = A_2 \\
\langle B_1|x|A_1\rangle &\rightarrow B_1 \times B_1 \times A_1 = A_1 \\
\langle B_1|y|A_1\rangle &\rightarrow B_1 \times B_2 \times A_1 = A_2 \\
\langle B_1|z|A_1\rangle &\rightarrow B_1 \times A_1 \times A_1 = B_1 \\
\langle B_2|x|A_1\rangle &\rightarrow B_2 \times B_1 \times A_1 = A_2 \\
\langle B_2|y|A_1\rangle &\rightarrow B_2 \times B_2 \times A_1 = A_1 \\
\langle B_2|z|A_1\rangle &\rightarrow B_2 \times A_1 \times A_1 = B_2
\end{aligned}$$

The matrix elements $\langle A_1|z|A_1\rangle$, $\langle B_1|x|A_1\rangle$ and $\langle B_2|y|A_1\rangle$ span A_1 and are therefore dipole allowed. One can also observe that there exists no transition $A_1 \rightarrow A_2$. This knowledge is helpful since it confirms that we can expect allowed transitions from O1s to the two LUMO:s $|O1s\rangle \rightarrow |4a_1\rangle$ and $|O1s\rangle \rightarrow |2b_2\rangle$. Using these results and now taking *eqn. 10* into account

$$P_{O1s\rightarrow 4a_1} \propto |\mathbf{e} \cdot \langle 4a_1|\mathbf{r}|O1s\rangle|^2. \tag{13}$$

The matrix element is only non-zero with $\mathbf{r} \parallel z$ and thus $P_{O1s\rightarrow 4a_1}$ has its largest amplitude with $e \parallel z$. By the same argument $P_{O1s\rightarrow 2b_2}$ has its largest amplitude with $e \parallel y$.

One thus knows that there exist a number of possible excitations. Connecting this knowledge to the absorption spectrum of H_2O in the relevant energy region helps us make the classification of states in *figure 5*.

It should be noted that gas-phase molecules have no fixed direction in space. Each molecule will thus occasionally align in the preferable direction with the linearly polarized light. The impact on the experiment is however that the momentum of the dissociation fragments will have a preferable direction for each excitation, which must be taken into account when constructing the setup.

B Appendix: An outlook on synchrotron light and the beamline technical details

B.1 Synchrotron light

A core-excitation of H_2O requires X-ray radiation on the order of 500 eV. The radiation needs to have a high photon flux and a well defined energy to allow only for electronic transitions to specific states. This is in practice only achievable at synchrotron radiation facilities.

Synchrotron radiation is produced when a beam of electrons is forced to move in accelerated motion. From Maxwell's equations one can deduce that a charged particle accelerated in any direction by an external force will emit light. Synchrotron

radiation was predicted 1898 by Alfred-Marie Liénard [28]. In theory, this was a well known phenomenon when the first electron accelerators were built. Nevertheless, it became a huge surprise for the technicians hwo first observed synchrotron radiation in 1947 [29]. For a device constructed to keep electrons at highest possible speed in circular motion this effect was a drawback, since the beam was drained of energy. However, the intense light produced as a by-product in these accelerators could itself be used for research. Today synchrotron radiation facilities are constructed only to achieve the best possible light for research.

Synchrotron radiation has some important properties. It is emitted in the direction of propagation of the electron beam, and its energy distribution is dependent on external electromagnetic forces. With a careful setup the synchrotron radiation can be made highly collimated (emitted in only one direction) and tuned (changing the energy). With enough charged particles at high velocity the photon flux can be made much higher than any other light source.

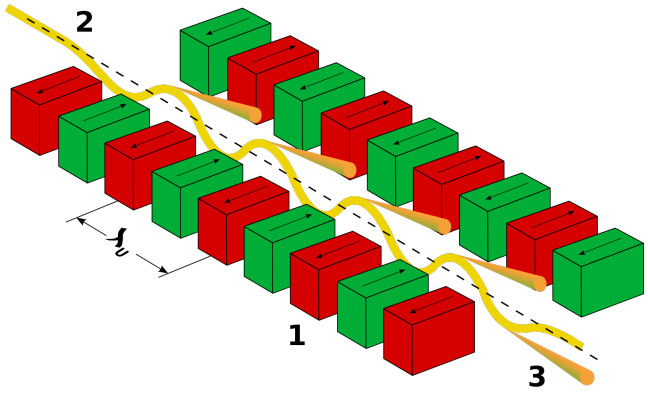

FIGURE 17 – *The working principle of an undulator. The incoming particle beam is forced to oscillate in a periodic magnetic field. The emitted light is defined by the undulator period length and the magnetic field between the magnetic arrays. By changing the distance of the arrays, the energy can be tuned. (Picture from Wikimedia Commons)*

A synchrotron radiation facility consists of a storage ring where electrons are forced to move in circular motion inside an evacuated tube. Ultra-high vacuum must be maintained within since otherwise the mean free path of the electrons would be too short. The ring lattice is the setup of all devices in a storage ring. It involves devices to bend the beam into a circular path — the *bending magnets* — and to focus the beam — the *quadrupole magnets*. Also the accelerating component — the *radio-frequency cavity* — and all insertion devices — *undulators* and *wigglers* — are included. These must be considered as a whole to make the structure work. They are not independent. Though a carefully designed array of magnets provides the necessary basis for good insertion devices.

A conventional undulator is a one-dimensional[11] array of alternating magnetic poles which are placed above and below the beam, causing the particle beam to oscil-

[11] Today there exist also undulators with other magnet setups, such as elliptically polarized undulators with two-dimensional arrays.

late (see *figure 17*). The light is emitted in the line of motion, i.e. straight forward. One can thus create a narrow cone of light. Furthermore, by allowing the distance of the arrays to be changed, the energy of the photons can be tuned. Due to interference effects, the emitted photon energies will be concentrated to emission peaks of certain calculable wavelengths.

High photon flux in narrow cones with well defined energy is very suitable for X-ray experiments. But to use the full potential of the light, further modification of the light is necessary.

B.2 The I411 beamline at MAX-lab

The experiments reported here have been performed at the I411 beam-line at MAX-lab in Lund [24]. The I411 beamline was originally situated at the MAX I storage ring. It was then known as BL-51 or the "Finnish beamline" [25]. Following the construction of MAX II the beamline was upgraded and moved to the new storage ring. The monochromator of BL-51 was kept on the 'new' beamline. The I411 beamline is designed for spectroscopic studies of gases, clusters, liquids and solids. It operates in the soft X-ray region, 50-1500 eV. It is permanently equipped with a Scienta SES-200 electron spectrometer at the end-station [26]. This end-station has not been used in these experiments. The spectrometer described in the following section were operated at the "one meter section" at the beamline. That means that the experiment is not performed at optimal focusing conditions. The beamline is constructed to give optimal focused light to the permanent endstation. The conditions at the one meter section are however sufficient for gas-phase experiments of this kind. The resolution deficiency of the un-focused light is smaller compared to other resolution limits connected to the experiment.

The beamline consists of the source and five optical elements. See illustration in *figure 18*. The optical data below and in the figure is drawn from Bässler et al [24] unless otherwise stated.[12]

Light source is an 2.65 m long undulator with 58.85 mm period, minimal gap 23 mm and $K_{max} = 3.6$.

M1 cylindrical premirror is the first mirror. It is focusing the beam horizontally on the monochromator exit slit. It performs no focusing in vertical direction. M1 takes on the biggest heat load and is thus water cooled. This and all following mirrors are gold coated.

SX 700 monochromator is a two-element movable system including the M2 plane mirror and grating. It is designed to enable monochromatization of light of a wide range of energies, keeping the beam on the same path[13]. M2 is simply reflecting the beam on the grating. The grating is blazed with 1221 lines per mm. The system elements are horizontal elements, thus performing vertical defocusing of the beam. The entrance arm is the full distance $r = 15000$ mm to the source (see *figure 18*). The angular magnification c [14] is fixed at 2.25, and thus the distance of the virtual source is $15000 \cdot 2.25^2 = 76588$ mm. The blaze angle is 1.35° [25].

[12] The text and calculations presented here are drawn upon a exercise made by the author during the course MAXM16 at MAX-lab, Lund University.

[13] So called fixfocus setting.

[14] Defined as $\cos\alpha / \cos\beta$ where α (β) is the incident (reflecting) angle.

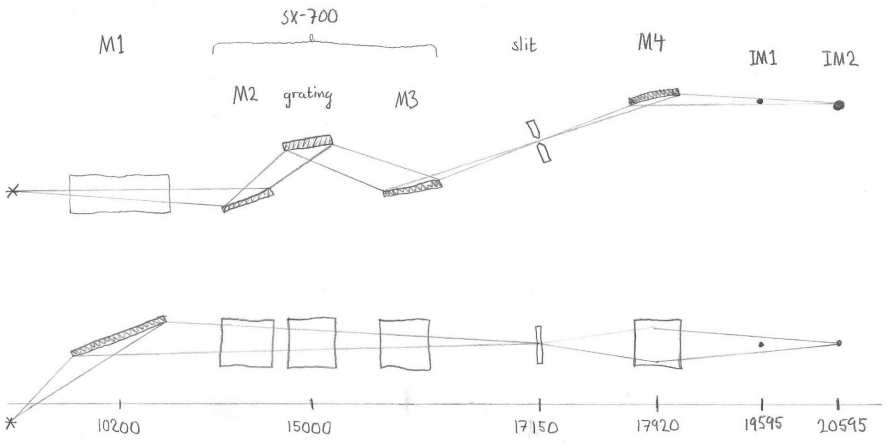

FIGURE 18 – *I411 beamline setup in side view (top) and top view (bottom). The experimental chamber is located at IM2. There is a possibitity to do experiments with other setups at IM1. (Illustration in Aksela et al [25] has been a great help producing this drawing.)*

M3 plane elliptical mirror performs the vertical focus on the exit slit. It takes the grating virtual source distance as entrance arm and the distance to the slit as exit arm. No focusing is performed horizontally. Since the publication [24] the mirror has been replaced with a better quality one. Slope errors have been reduced to 0.09" meriodinal and 0.19" sagital [19].

Slit takes a vertical slice of the beam. Note that the slit is in the foci of both directions (M1 focus horizontally and M3 focus vertically on the slit).

M4 toroidal mirror focuses the beam in both directions on the experimental chamber (IM2 in *figure 18*). The entrance arms are however not equal due to a optimization where the vertical and horizontal beam waist (the narrowest point) were used as focus points rather than the slit position. In vertical (meriodinal) direction the entrance arm was only extended by a few mm, though the horizontal (sagital) entrance arm was extended with 3.5 m. The authors of [24] describes this as an effect of the low emittance and the source size of the beam.

A model of the I411 beamline has been made in the BESSY raytrace program RAY [27]. Calculations of spot size (*figure 19*) and energy distribution (*figure 20*) at 500 eV light and 10 μm has been made at IM1.

C Appendix: An outlook on the PEPICO spectrometer technical details

The PEPICO setup was designed and described by Kukk et al [18]. It consists of a Scienta SES-100 hemisperical electron analyser and a ion time-of-flight spectrometer.

In a homogeneous electric field a charged particle experiences a constant force parallel or anti-parallel to the field vector. These particles are subject to acceleration

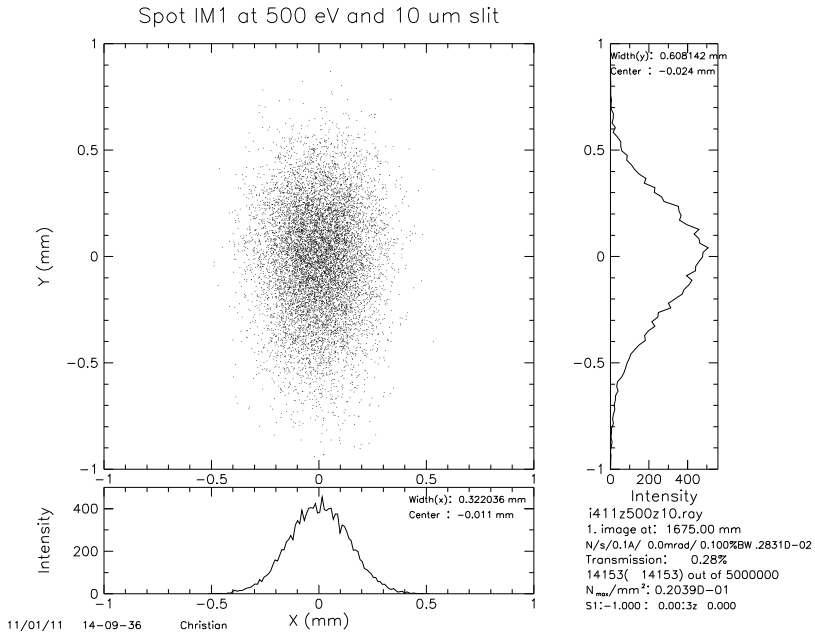

FIGURE 19 – *Spot size on sample at IM1 calculated for 500 eV light. The spot size is one the mm-scale.*

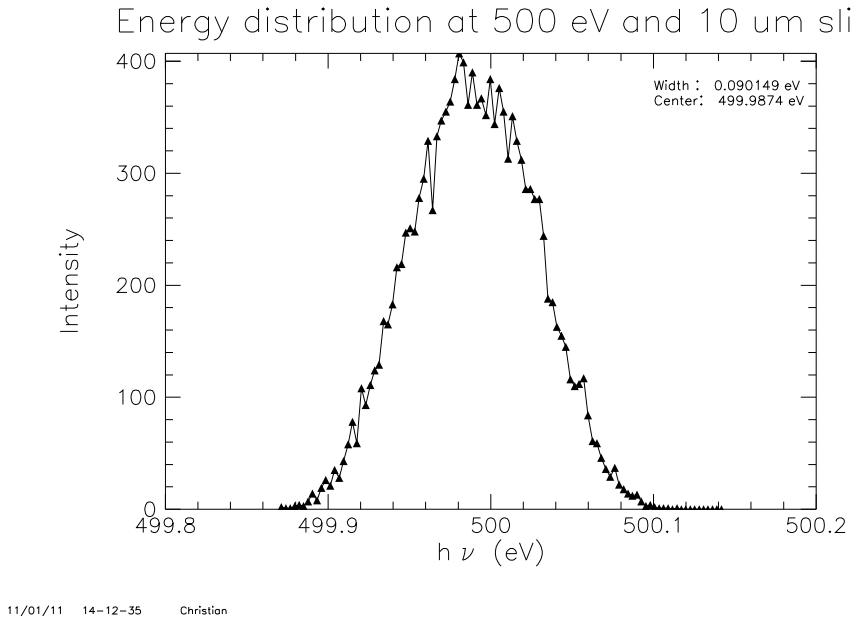

FIGURE 20 – *Energy distribution at sample calculated for 500 eV light and 10 μm slit size. The bandwidth is ≈ 0.2 eV.*

according to Newton's second law for the accelerating force $F_{acc} = ma$ and the definition of the electric force $F_e = Eq$ where E is the electric field. For $F_{acc} = F_e$ (only electric forces present) the acceleration will be inversely proportional to their mass-to-charge ratio $a \propto (m/q)^{-1}$. Thus, the time it takes for a particle with zero initial kinetic energy to travel a certain distance in a homogeneous electric field will be solely determined by the mass-to-charge ratio of that particle. For convenience the mass-to-charge ratio is given in units of u/e where 1 u is the unified atomic mass unit and e is the elementary charge. In this unit e.g. the O^+ ion would have mass-to-charge ratio 16 and OH^{2+} would have 8.5. This argument allows us to use time-of-flight. If the initial kinetic energy of a certain ion is sufficiently low, all ions of that kind have the same TOF. Hence, one is able to use TOF-spectrometers to evaluate the mass-to-charge ratio of an unknown particle.

In this setup the electron detection trigger is used as a clock-starter. The clock stops when an ion is recorded on the ion detector. The detector can record a series of ion hits with a very small dead-time between the events. The ability to record and analyze two photo-ions in coincidence with a photoelectron is called *photoelectron photo-ion photo-ion coincidence spectroscopy (PEPIPICO)*. Two photo-ions will of course only occur if the process creates at least two cation fragments.

The TOF-spectrometer is of Wiley-McLaren type [31]. The extraction region is followed by a acceleration region and a drift tube. The 10 mm long extraction region is applied with a voltage. The following 392 mm long drift tube is without electric field. Its purpose is to extend the effect of the acceleration region. The active area of the detector consist of a 40 mm wide multi-channel plate. The detector can to some extent measure the position of the ion hit, but this will not be further explored here.

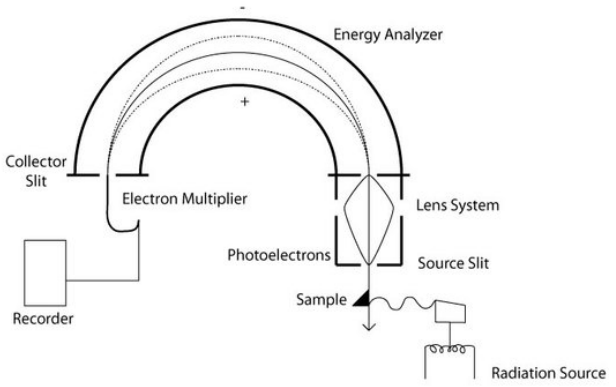

FIGURE 21 – *Schematic layout of a typical hemispherical electron analyzer. (Picture: Jessica Woods)*

The Scienta SES-100 electron energy analyser [32] provides a possibility to detect electrons and measure their energy. The working principle of an hemispherical electron analyser is that a bundle of charged particles with equal energy originating from a point at the entrance of a perfect half-sphere condenser (see *figure 21*) with proper applied charges will be focused to one point at the exit of the half sphere, a theorem proven by Purcell in 1938 [33]. Electrons with equal energy will thus be focused on

the same spot even if they have angular spread from the point of origin. This feature allows a properly charged condenser to act as a electron energy analyser. If a detector is placed at the focus point it will register only electrons with a specific energy. The SES-100 analyser has been equipped with a resistive anode position-sensitive detector [18]. The position-sensitive feature allows for detection of a certain range of electron energies. When an electron has slightly lower energy, it will experience more deflection and thus appear at the detector at a point closer to the source; if the energy is higher the opposite is true. With calibration we are able to deduce from the position of the hit which energy the electron had.

It has been recalled by Field and Eland [30] that there is a conflict between good electron energy resolution and good ion energy resolution since the former is in need of a weak extraction field and the latter requires the opposite. The proposed solution, which is implemented in our setup, is to use pulsed extraction field mode as described above. However this setup requires proper timing and careful setup of electronics. It is unavoidable that the extraction pulse will have a delay following the electron detection. In this setup the delay is set to be 1 μs.

The energy resolution of the electron analyser is determined by applied potentials on the condenser and the pass energy. The number of channels on the detector plate are limited. As one converts distance on the plate to electron energy the resolution will be proportional to the energy range one is measuring. If the analyser is set so that the detector accepts a larger range of electron energies the resolution will thus decline. The detectable energy range is determined by the pass energy of the hemisphere, basically the potential on the halfsphere condenser. The energy range is always approximately one tenth of the pass energy. To enable tuning of the analyser a decelerating electric field can be applied before the entrance of the halfsphere. Measuring the energy of electrons in the vicinity of 500 eV can thus be performed either with high lens fields and low pass energy or vice versa, the former giving a large energy range but bad resolution.

Total resolution of the electron energy is a convolution of many individual broadening effects. The *natural broadening* is a intrinsic effect of the Heisenberg uncertainty relation showing that if the electron is produced from the decay of an intermediate state with short life-time the energy of that electron will be more uncertain and thus broadened. *Thermal broadening* comes from the motions of particles in the interaction region. It is in the order of kT 0.01 eV in room temperature. One effect is the deviation of photon energies from the synchrotron light source. However, the all over-shadowing effect determining resolution in this experiment will be the detector resolution. The choice of low detector resolution is determined by our absolute need to measure as many electrons as possible, and also electrons in a reasonably large energy range to include all resonant Auger electron energies of a transition.

The gross structure of the TOF spectrum is determined by the mass-to-charge ratio of the fragments. Broadening effects will be present depending on the speed of the charged fragments after fragmentation. Fragments dissociating in a process where kinetic energy is deployed on it can have a initial velocity parallell or anti-parallell to the spectrometer axis. In the former case the arrival to the detector will be earlier, and vice versa.

D Populärvetenskaplig sammanfattning (in Swedish)

Sönderslagning av vattenmolekyler med hjälp av intensivt ljus har genom historien haft mycket stor påvekan på människan och världen. Vatten finns överallt omkring oss, och så har det varit under nästan hela jordens historia. När liv uppstod på jorden för 3,5 miljarder år sedan skedde det troligen i vatten. Detta var under en tid i jordens historia när strålningen från solen var mycket stark, och fragment från vattenmolekyler måste ha varit delaktiga i kemiska processer när livets molekyler bildades. Detta examensarbete undersöker hur det går till när kemiska bindningar i vattenmolekylen bryts på grund av intensiv röntgenstrålning. Jag har studerat vilka slutprodukter som bildas och hur mycket energi de bär med sig. Jag har kunnat visa att vattenmolekylen i vissa fall splittras extremt fort, hela processen tar bara ett par femtosekunder (alltså 0,000 000 000 000 001 sekunder). På den tidsskalan frigörs väte direkt från vattenmolekylen.

Vattenmolekylen, som är den minsta byggstenen i vatten, består av två väteatomer och en syreatom. Atomerna är hårt bundna till varandra. När vattenmolekylen bryts sönder bildas mindre fragment. Dessa fragment kan bestå av ensamma syre- och väteatomer, men också molekyler med en väteatom och en syreatom som sitter ihop. En av produkterna man kan få av vattenmolekyer är vätgas. Väteatomerna, som är mycket små och lätta, är en tiondel av vattnets vikt. Vätgas kan separeras från vattenmolekylen genom kemiska reaktioner. Redan idag finns det bilar och bussar som tankas med vätgas istället för bensin, etanol och biogas. Vätgasmotorn, också kallad bränslecell, har den enorma fördelen att den inte släpper ut andra avgaser än vatten. Ett perfekt scenario vore om man kunde använda solljus för att skilja ut vätgas från vatten och tanka bilarna med. Det skulle vara ett slutet kretslopp av vatten drivet av förnyelsebar solenergi. En av utmaningarna är att hitta ett effektivt sätt att skilja ut vätgasen från vatten.

För att få väte att släppa från vattenmolekylen måste man påverka de bindningar som håller ihop molekylen. En vattenmolekyl är mycket stabil, men ljus och strålning kan påverka dess inre struktur. Den kan byta form. Om man väljer strålning med rätt energi kan en bindning brytas och en väteatom blir fri. Fria väteatomer betyder att man kan utvinna vätgas. Den avgörande frågan är då när ljuset eller strålningen har precis den energi som behövs.

I detta examensarbete har jag specifikt undersökt vad som händer när man bestrålar vattenmolekyler med röntgenstrålning med olika energi. En röntgenstråle är en mycket intensiv stråle av ljuspartiklar, fotoner. Varje foton bär med sig en liten men mycket bestämd mängd energi. När en lämplig foton träffar en vattenmolekyl kan molekylen ta över fotonens energi. Man säger att vattenmolekylen hamnar i ett högre energitillstånd. När en molekyl har överskottsenergi gör den sig snabbt av med den. Den kan göra sig av med en partikel, ofta en foton eller en elektron. Ibland gör sig syreatomen av med en eller båda sina väteatomer. Det experiment som jag har gjort mäter när detta händer och exakt hur fragmenten ser ut.

Experimentet gjordes på forskningsanläggningen MAX-lab. Där kan vi generera en mycket stark röntgenstråle där alla fotoner har den energi som vi bestämmer. Det betyder att när en vattenmolekyl träffas av fotonen vet vi precis hur mycket överskottsenergi molekylen får. Vi varierar energin och mäter samtidigt hur molekylen beter sig. När molekylen gör sig av med en elektron så mäter vi dess hastighet. Samtidigt mäter vi vilka fragment som bildas. Man kan alltså mäta om vi får fria väteatomer eller inte. Farten på elektronen gör att vi kan se hur mycket överskottsenergi som finns kvar i fragmenten. All denna information är pusselbitar i ett detekti-

varbete där experimentets resultat ska kopplas till teoretiska beräkningar av hur en vattenmolekyl sitter ihop. Man kan säga att vi plockar isär vattenmolekylen för att se hur den ser ut på insidan.

Trots att vattenmolekylen är världens mest studerade molekyl så är den fortfarande ett mysterium. Hur kan det komma sig att vatten är det perfekta ämnet för livet här på jorden? Svaren på denna gåta kanske vi i framtiden kan finna när vi studerar dess minsta beståndsdelar, molekyler och atomer.

References

[1] Empedokles. http://www.ne.se/lang/empedokles, *Nationalencyklopedin*, 2011-03-25.

[2] I. Hjelte, M. N. Piancastelli, R. F. Fink, O. Björneholm, M. Bässler, R. Feifel, A. Giertz, H. Wang, K. Wiesner, A. Ausmees, C. Miron, S. L. Sorensen and S. Svensson, *Chem. Phys. Lett.* **334** (2001) 151-158

[3] R. Feifel, M.N. Piancastelli, *J. Electron Spectrosc. Relat. Phenom.* **183** (2011) 10

[4] B. H. Bransden and C. J. Joachain (1983), *Physics of Atoms and Molecules*, (Longman Scientific & Technical, Harlow, UK)

[5] P. Atkins and R. Friedman (2011), *Molecular Quantum Mechanics (fifth edition)*, (Oxford University Press, Oxford, UK)

[6] H. M. Randall, *Rev. Mod. Phys.* **10** (1938) 72

[7] R. T. Hall and J. M. Dowling, *J. Chem. Phys.* **47** (1967) 2454

[8] B. T. Darling and D. M. Dennisson, *Phys. Rev.* **57** (1940) 128

[9] D. Chattarji (1976), *The theory of Auger Transitions*, (Academic Press, London, UK)

[10] R. S. Mulliken, *J. Chem. Phys.* **23** (1955) 1997

[11] D. Attwood (2000), *Soft X-rays and extreme ultraviolet radiation : principles and applications*, (Cambridge University Press, Cambridge, UK)

[12] A. Naves de Brito, R. Feifel, A. Mocellin, A. B. Machado, S. Sundin, I. Hjelte, S. L. Sorensen and O. Björneholm, *Chem. Phys. Lett.* **309** (1999) 377

[13] M. Eroms, O. Vendrell, M. Jungen, H.-D. Meyer and L. S. Cederbaum, *J. Chem. Phys.* **130** (2009) 154307

[14] A. Lindgren, *Ion Spectroscopic Measurements on photo-aligned small molecules*, (MediaTryck, Lund University, Lund, 2006), pp. 8-10

[15] H. Siegbahn, L. Asplund and P. Kelfve, *Chem. Phys. Lett.* **35** (1975) 330

[16] M. N. Piancastelli, A. Hempelmann, F. Heister, O. Gessner, A. Rüdel and U. Becker, *Phys. Rev. A* **59** (1999) 300

[17] I. Hjelte, M.N. Piancastelli, C.M. Jansson, K. Wiesner, O. Björneholm, M. Bässler, S.L. Sorensen, S. Svensson, *Chem. Phys. Lett.* 370 (2003) 781

[18] E. Kukk, R. Sankari, M. Huttula, A. Sankari, H. Aksela and S. Aksela, *J. Electron. Spectrosc. Rel. Phenom.* **155** (2007) 141-147

[19] Direct contact with associate senior lecturer Rami Sankari (MAX-lab, Lund university)

[20] G. C. King, M. Tronc, F. H. Read and R. C. Bradford, *J. Phys. B* **10** (1977) 2479

[21] I. Hjelte, L. Karlsson, S. Svensson, A. De Fanis, V. Carravetta, N. Saito, M. Kitajima, H. Tanaka, H. Yoshida, A. Hiraya, I. Koyano, K. Ueda and M. N. Piancastelli, *J. Chem. Phys.* **122** (2005) 084306

[22] www.molcas.org

[23] O. Takahashi, M. Odelius, D. Nordlund, A. Nilsson, H. Bluhm and L. G. M. Pettersson, *J. Chem. Phys.* **124** (2006) 064307

[24] M. Bässler, A. Ausmees, M. Jurvansuu, R. Feifel, J.-O. Forsell, P. de Tarso Fonseca, A. Kivimäki, S. Sundin, S.L. Sorensen, R. Nyholm, O. Björneholm, S. Aksela and S. Svensson, *Nuclear Instruments and Methods in Physics Research A*, **469** (2001), 382-393

[25] S. Aksela, A. Kivimäki, A. Naves de Brito, O.-P. Sairanen, S. Svensson and J. Väyrynen, *Rev. Sci. Instrum.*, **65** (1994), 831-836

[26] N. Mårtensson, P. Baltzer, P.A. Bruhwiler, J.-O. Forsell, A. Nilsson, A. Stenborg and B. Wannberg, *J. Electron Spectrosc. Relat. Phenom.* 70 (1994) 117

[27] F. Schäfers (2008) The BESSY Raytrace Program RAY. In A. Erko, M. Idir, Th. Krist and A. G. Michette (Eds.) *Modern Developments in X-ray and Neutron Optics* (Springer Verlag, Berlin Heidelberg)

[28] A. Liénard, *L'Eclairage Elec.* **16** (1898) 5

[29] H. C. Pollock, *Am. J. Phys.* **51** (1983) 278

[30] T. A. Field and J. H. D. Eland, *Meas. Sci. Technol.* **9** (1998) 922

[31] W. C. Wiley and I. H. McLaren, *Rev. Sci. Instrum.* **26** (1955) 1150

[32] M.Huttula, S. Heinasmaki, H. Aksela, E. Kukk and S. Aksela, *J. Electron. Spectrosc. Rel. Phenom.* **156-158** (2007) 270-273

[33] E. Purcell, *Phys. Rev.* **54** (1938) 818